

Understanding the state-dependent impact of species correlated responses on community sensitivity to perturbations

Lucas P. Medeiros  | Serguei Saavedra 

Department of Civil and Environmental Engineering, Massachusetts Institute of Technology, Cambridge, Massachusetts, USA

Correspondence

Lucas P. Medeiros
Email: lumedeir@ucsc.edu

Present address

Lucas P. Medeiros, Institute of Marine Sciences, University of California Santa Cruz, Santa Cruz, California, USA.

Funding information

Martin Family Society of Fellows for Sustainability; MIT Sea Grant Program; National Science Foundation, Grant/Award Number: DEB-2024349

Handling Editor: Tadashi Fukami

Abstract

Understanding how communities respond to perturbations requires us to consider not only changes in the abundance of individual species but also correlated changes that can emerge through interspecific effects. However, our knowledge of this phenomenon is mostly constrained to situations where interspecific effects are fixed. Here, we introduce a framework to disentangle the impact of species correlated responses on community sensitivity to perturbations when interspecific effects change over time due to cyclic or chaotic population dynamics. We partition the volume expansion rate of perturbed abundances (community sensitivity) into contributions of individual species and of species correlated responses by converting the time-varying Jacobian matrix containing interspecific effects into a time-varying covariance matrix. Using population dynamics models, we demonstrate that species correlated responses change considerably across time and continuously alternate between reducing and having no impact on community sensitivity. Importantly, these alternating impacts depend on the abundance of particular species and can be detected even from noisy time series. We showcase our framework using two experimental predator-prey time series and find that the impact of species correlated responses is modulated by prey abundance—as theoretically expected. Our results provide new insights into how and when species interactions can dampen community sensitivity when abundances fluctuate over time.

KEY WORDS

Jacobian matrix, population dynamics, population fluctuations, species interactions, stability, time series

INTRODUCTION

Natural and human-driven perturbations such as fires (Cochrane, 2003), storms (Turner et al., 1997), pollution (Carpenter et al., 1998), and overfishing (Jackson et al.,

2001) can alter the composition of ecological communities and the abundance of their constituent species. Thus, there is an urgent need to understand the capacity of communities to retain their biodiversity and functioning in the face of rapidly increasing perturbations (Cardinale

This is an open access article under the terms of the [Creative Commons Attribution-NonCommercial-NoDerivs License](#), which permits use and distribution in any medium, provided the original work is properly cited, the use is non-commercial and no modifications or adaptations are made.

© 2023 The Authors. *Ecology* published by Wiley Periodicals LLC on behalf of The Ecological Society of America.

et al., 2012; Levin & Lubchenco, 2008). It is well known that the way communities respond to perturbations (e.g., recovery, constancy, sensitivity) cannot be explained solely by the sum of responses of isolated species but depends crucially on the interactions among these species (Kéfi et al., 2019; Pennekamp et al., 2018; Pimm, 1984; Tilman et al., 2006). Indeed, because not all species are equal and species may affect each other's responses, scaling up from individual species through their interactions to understand the response of an entire community to perturbations remains an important challenge.

A fundamental consequence of species interactions is that changes in the abundance of a given species following a perturbation may cascade and shift the abundance of other species, creating correlations in how species respond to perturbations. Such correlated responses include, for example, shifts in prey (or resources) immediately following changes in the abundance of predators (or consumers) (Dulvy et al., 2000; Estes et al., 1998; Pringle et al., 2007) and shifts in competitors immediately following changes in environmental conditions (Brown et al., 2016; Fischer et al., 2001; Tilman et al., 2006). Importantly, such correlations can impact the response of aggregate community properties following perturbations. For instance, when measuring community response as the constancy of total abundance over time, opposite changes in the abundance of different species (i.e., negative correlations) will increase community constancy—a phenomenon known as compensatory dynamics (Brown et al., 2016; Fischer et al., 2001; Gonzalez & Loreau, 2009; Tilman et al., 2006). Given that many ecosystem services depend on total abundance, compensatory dynamics has been invoked as a central mechanism stabilizing the provision of these services (Cardinale et al., 2012; Gonzalez & Loreau, 2009).

Despite important progress in assessing how species correlated responses affect whole-community response to perturbations, the fact that this effect appears to be context-dependent has posed significant challenges to its understanding. Key examples come from food web studies, where the effect of removing or adding a predator on other species in the community critically depends on the sign and strength of species interactions (Samhouri et al., 2017; Schneider et al., 2012; Worsfold et al., 2009). Thus, depending on species' initial abundances and their interactions, two species may show a positive, negative, or null correlation in their response to a perturbation. Such context dependency becomes clearer when we consider that in many natural communities, the local effect of each species on the growth rate of other species in the community (hereafter interspecific effects) shifts over time due to changes in community state (i.e., distribution of species abundances) (Deyle et al., 2016; Ushio et al., 2018). That is,

even when the sign and strength of the per-capita effect of a species on the per-capita growth rate of another species is fixed (e.g., fixed interaction parameters in a population dynamics model), interspecific effects (i.e., elements of the Jacobian matrix of a model) will change when species abundances change (Medeiros et al., 2021; Song & Saavedra, 2021). The fact that interspecific effects are state-dependent is particularly important when populations do not settle down to a fixed point (e.g., transient, cyclic, or chaotic dynamics), which is the case for many communities (Becks et al., 2005; Begon et al., 1996; Blasius et al., 2020; Deyle et al., 2016; Hastings et al., 2018; Ushio et al., 2018). What is currently unknown is how such interspecific effects shape species correlated responses to perturbations and, in turn, how such correlations impact whole-community response when populations exhibit deterministic fluctuations over time around an attractor (e.g., limit cycles, chaos) or when they undergo transient dynamics before they reach an equilibrium.

Moving beyond the typical assumption of populations at a fixed point, recent work has begun to elucidate how communities respond to perturbations when populations fluctuate over time. For example, it has been shown that, not only interspecific effects but also a community's response to perturbations change over time when dynamics are in equilibrium but undergo a cyclic or chaotic behavior (Cenci & Saavedra, 2019; Rogers et al., 2023; Ushio et al., 2018). In particular, such a community may have a time-varying sensitivity to changes in environmental conditions (Cenci et al., 2020; Cenci & Saavedra, 2019). In addition to whole-community response, the sensitivity of individual species to perturbations has also been shown to change over time, implying that the identity of the most sensitive species also depends on community state (Medeiros et al., 2023). In spite of this recent progress, current frameworks to quantify response to perturbations at the community (Cenci & Saavedra, 2019) and species levels (Medeiros et al., 2023) have remained disconnected. However, investigating potential time-varying correlations in how species respond to perturbations may provide the key to understanding the links between responses to perturbations at these two levels of biological organization.

Here we introduce a theoretical framework to assess the time-varying impact of species correlated responses (hereafter species correlations) on the sensitivity of a community to perturbations. In what follows, we first present our framework, which consists of partitioning community sensitivity—measured as the volume expansion rate of perturbed abundances—into contributions of individual species and of species correlations by converting the time-varying Jacobian matrix into a

time-varying covariance matrix. Then we illustrate our framework using synthetic time series generated from population dynamics models and show how we can identify community states where species correlations have either a weak or strong impact on community sensitivity. Our conceptual framework is general to any type of deterministic dynamics (e.g., fixed points, transient dynamics, limit cycles, chaotic dynamics). However, in practice, we focus on cases where a community has had enough time to approach an attractor because the statistical approach we use to infer the time-varying Jacobian matrix requires population dynamics around an attractor (*Materials and methods*). Lastly, we apply our framework to two experimental predator–prey communities and find that prey abundance is an important factor determining whether or not species correlations can dampen community sensitivity to perturbations over time.

RESULTS

Species correlations and their impact on community sensitivity

In general, the population dynamics of a community with S species can be written $\frac{d\mathbf{N}}{dt} = \mathbf{f}(\mathbf{N})$, where $\mathbf{N} = [N_1, \dots, N_S]^\top$ is the vector of species abundances and $\mathbf{f} = (f_1, \dots, f_S)$ ($f_i: \mathbb{R}^S \rightarrow \mathbb{R}$) is a set of generic functions describing abundance growth rates (Case, 2000). As an example, consider a model of a community with one predator and one prey (*Materials and methods*; Equation 2). Under certain parameter values, this model generates a limit cycle, which we use to illustrate the state-dependent impact of species correlations on whole-community sensitivity to perturbations (Figure 1). At any given state (i.e., any \mathbf{N} along the cycle), this community may be affected by a pulse perturbation $\mathbf{p} = [p_1, \dots, p_S]^\top$ that changes \mathbf{N} into $\tilde{\mathbf{N}}$ (i.e., $\tilde{\mathbf{N}} = \mathbf{N} + \mathbf{p}$) (Bender et al., 1984). The vector $\tilde{\mathbf{N}}$ would then change in time according to \mathbf{f} . For instance, consider a perturbation that decreases the abundance of the predator ($\mathbf{p} = [-7, 0]^\top$, red arrow in Figure 1a,b) and an opposite perturbation with the same magnitude ($\mathbf{p} = [7, 0]^\top$, blue arrow in Figure 1a,b). Figure 1a shows the impact of these two perturbations on the prey abundance (ΔN_2) at time t_1 and after k time steps. The figure shows that, although one perturbation decreased the predator abundance and the other increased it, the impacts on the prey abundance (red ΔN_2 vs. blue ΔN_2 in Figure 1a) are similar to each other. Thus, knowing how the perturbation affects the predator conveys little information about the amount of change in the prey (i.e., species responses to

perturbations are uncorrelated). Interestingly, however, the same perturbations applied at time t_2 can trigger a completely different outcome (Figure 1b). Figure 1b shows that the impact on prey abundance is much greater when the predator abundance is decreased (red ΔN_2 in Figure 1b) than when it is increased (blue ΔN_2 in Figure 1b). In this case, knowing how the perturbation impacts the predator gives information about how much change we are likely to see in the prey (i.e., species responses to perturbations are correlated).

Although the previous example is based on only two perturbations (decreasing or increasing the predator abundance), we can observe the same outcomes when considering several random perturbations \mathbf{p} around \mathbf{N} (Figure 1c,d). Note that here we focus on random perturbations as we typically have no a priori information about how much an external perturbation will affect each species in a community. Each light purple point in Figure 1c,d represents a vector of perturbed abundances ($\tilde{\mathbf{N}}$; total of 200 vectors), where $p_i \sim \mathcal{N}(\mu = 0, \sigma^2 = 9)$. Figure 1c shows the distribution of perturbed abundances at t_1 (light purple points) and after k time steps (dark purple points). As expected from Figure 1a, the correlation between \tilde{N}_1 and \tilde{N}_2 (computed from all 200 perturbed abundances) at $t_1 + k$ is almost zero ($\rho = 0.01$; Figure 1c). Similarly, Figure 1d shows the distribution of perturbed abundances at t_2 (light purple points) and after k time steps (dark purple points). As expected from Figure 1b, the correlation between \tilde{N}_1 and \tilde{N}_2 at $t_2 + k$ is strong and negative ($\rho = -0.76$; Figure 1d). This numerical exercise illustrates the main question we address in this study: How does the absence (Figure 1c) or presence (Figure 1d) of species correlations at different community states impact whole-community sensitivity to perturbations?

Decomposing community sensitivity to perturbations

When a community is at a stable fixed point, that is, $\mathbf{N} = \mathbf{N}^*$ with $\mathbf{f}(\mathbf{N}^*) = \mathbf{0}$, the response of a community to pulse perturbations has been studied using several different indicators such as recovery rate (Arnoldi et al., 2018) and reactivity (Neubert & Caswell, 1997). Nevertheless, when communities are under cyclic or chaotic dynamics, it is necessary to establish a measure of community response that does not depend on a return to a fixed point. Therefore, here we focus on a measure known as the volume expansion rate, which is related to how much change we expect to see in \mathbf{N} under perturbations—that is, the community sensitivity to perturbations (Figure 2a) (Cenci et al., 2020; Cenci & Saavedra, 2019). Although this measure was originally used to measure sensitivity to

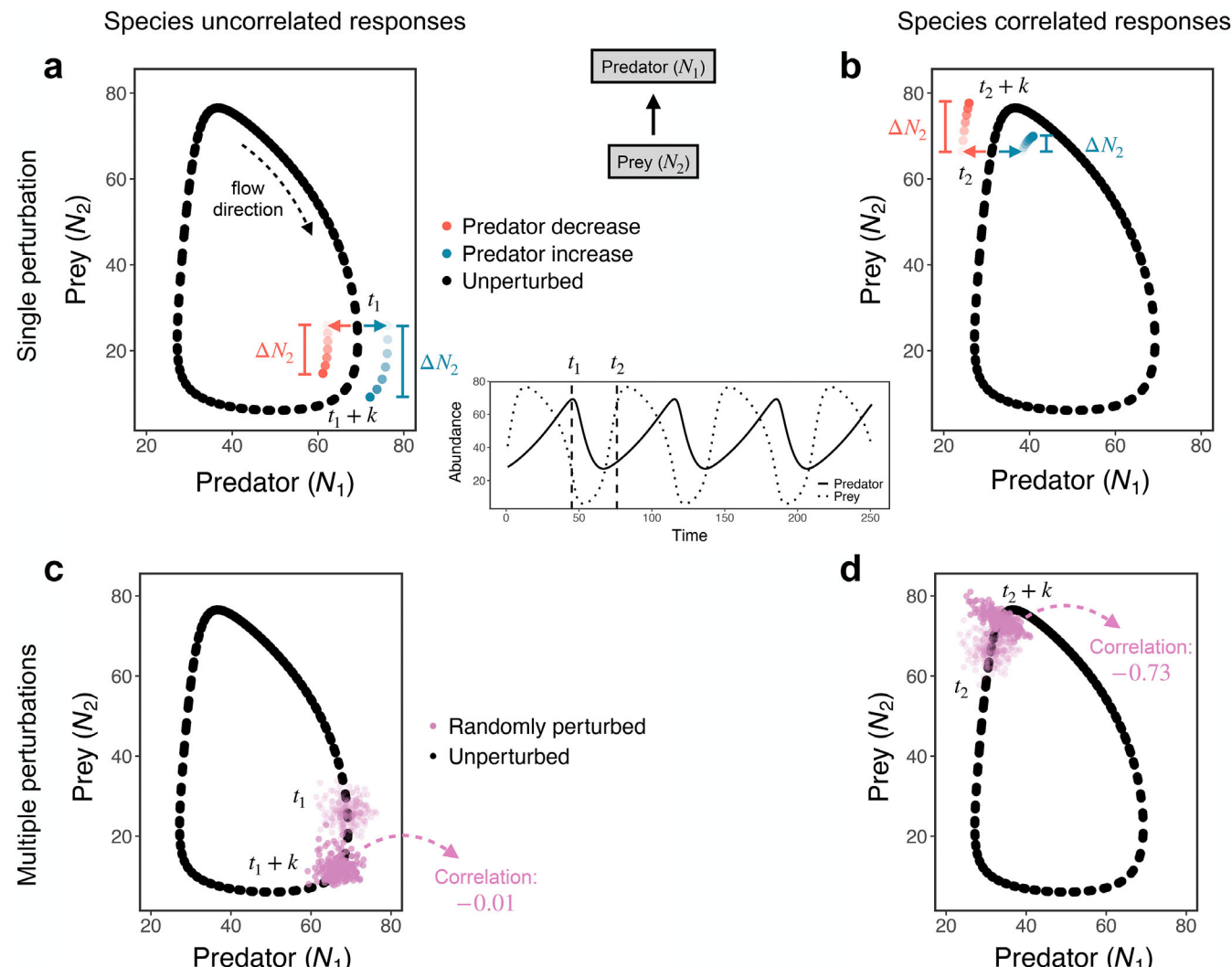


FIGURE 1 Correlations in how species respond to perturbations depend on community state. (a, b) Limit cycle of a two-species predator-prey model (black points; Equation 2) with two pulse perturbations ($\mathbf{p} = [-7, 0]^\top$: red arrow; $\mathbf{p} = [7, 0]^\top$: blue arrow) affecting the abundance of the predator (N_1) at two different points in time (t_1 and t_2). The middle panel shows the abundance time series (solid line: predator; dotted line: prey) and the two time points as vertical dashed lines. (a) At time t_1 , the effect of both perturbations on prey abundance after $k = 3$ time steps (ΔN_2) is similar ($\Delta N_2 = -11.1$ when predator decreases, in red; $\Delta N_2 = -16.7$ when predator increases, in blue). (b) In contrast, at time t_2 , one perturbation has a much greater effect on prey abundance than the other ($\Delta N_2 = 11.2$ when predator decreases, in red; $\Delta N_2 = 3.5$ when predator increases, in blue). (c, d) Same limit cycle as in (a) and (b) but showing the outcome of multiple random perturbations ($p_i \sim \mathcal{N}(\mu = 0, \sigma^2 = 9)$) that change \mathbf{N} (black point) into $\tilde{\mathbf{N}}$ (light purple points) at times t_1 (c) and t_2 (d). (c) At time $t_1 + k$, there is no correlation between the perturbed abundances of the predator (\tilde{N}_1) and of the prey (\tilde{N}_2) (dark purple points; correlation: -0.01). (d) In contrast, at time $t_2 + k$, there is a strong correlation between the perturbed abundances of the predator and of the prey (dark purple points; correlation: -0.73).

perturbations on the parameters of population dynamics (Cenci & Saavedra, 2019), we prove that this measure is also informative about perturbations on species abundances (*Materials and methods*). In what follows, we derive our framework of partitioning community sensitivity into contributions of individual species and of species correlations.

Because we typically have no information about the effect of external perturbations, here we assume that pulse perturbations at an arbitrary time $t(\mathbf{p}(t))$ follow a

distribution with mean vector μ_t and covariance matrix Σ_t (Figure 2a; *Materials and methods*). Using the linearized dynamics of \mathbf{p} , we can then obtain the covariance matrix of $\mathbf{p}(t+k)$ as $\Sigma = e^{k\mathbf{J}}\Sigma_t e^{k\mathbf{J}^\top}$ (Appendix S1: Section S1). Thus, Σ is obtained via a transformation of the initial covariance matrix (Σ_t) due to interspecific effects present in the Jacobian matrix \mathbf{J} (Figure 2a). We assume that \mathbf{J} is almost constant from time t to $t+k$, which is a reasonable assumption whenever k or $\frac{d\mathbf{N}}{dt}$ is small (Medeiros et al., 2023). Note, however, that \mathbf{J} is evaluated

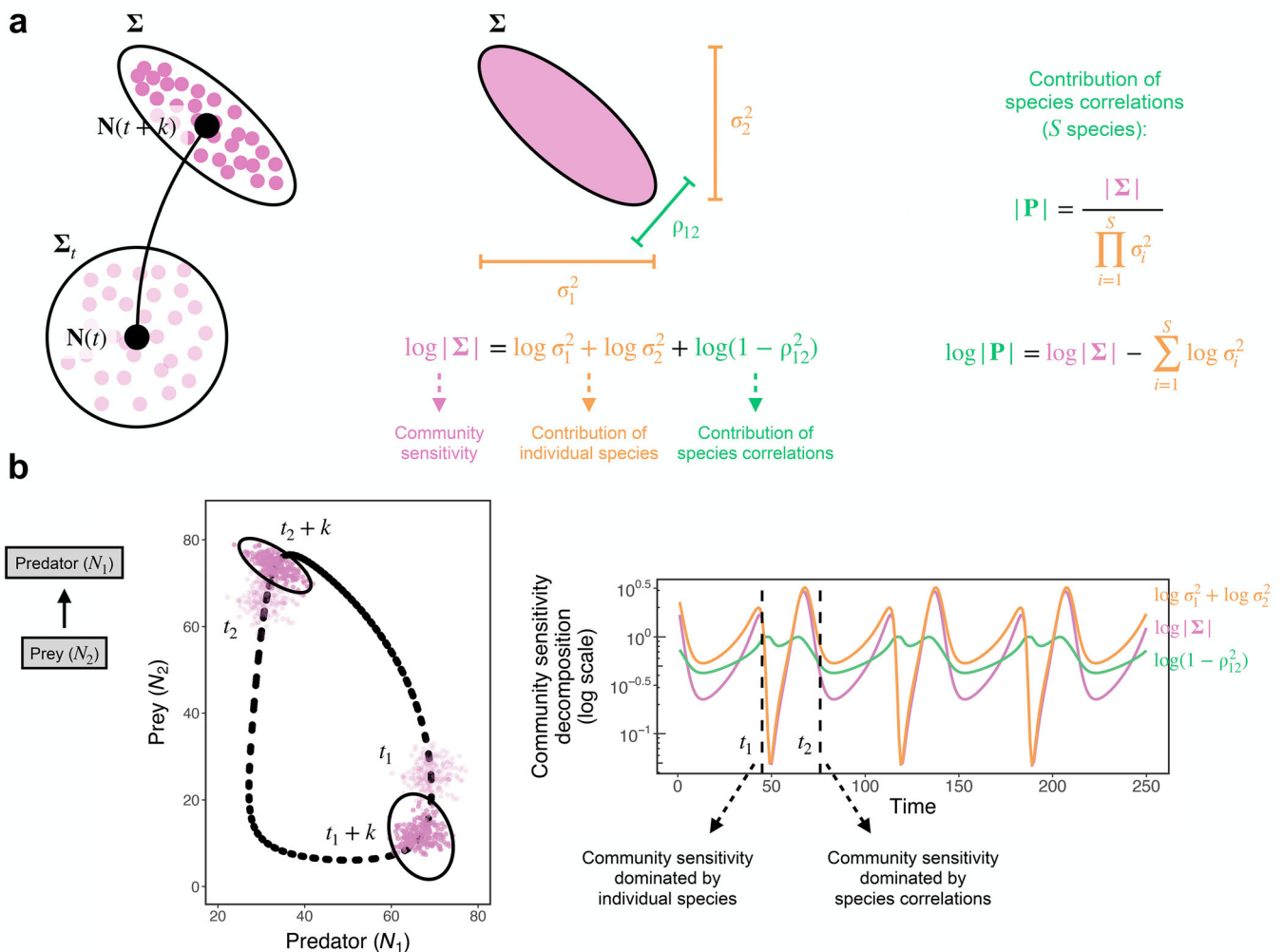


FIGURE 2 Decomposing community sensitivity into contributions of individual species and of species correlated responses. (a) (left) Diagram of a trajectory showing how perturbed abundances at time t (light purple points) generated using covariance matrix Σ_t (black circle) can be described at time $t+k$ (dark purple points) by covariance matrix Σ (black ellipse). (a) (center) Decomposition of community sensitivity to perturbations (volume expansion rate, $\log |\Sigma|$) into contributions of individual species (variances in Σ , $\sum_{i=1}^S \log \sigma_i^2$) and of species correlations (determinant of correlation matrix, $\log |\mathbf{P}|$), which is shown for two species. (a) (right) With S species, we can compute the ratio $|\mathbf{P}| = \frac{|\Sigma|}{\prod_{i=1}^S \sigma_i^2}$, where $|\mathbf{P}| \rightarrow 0$ indicates that community sensitivity is minimized due to species correlations. (b) (left) Same predator-prey limit cycle (black points; Equation 2) and time points (t_1 and t_2) as in Figure 1 showing that Σ (black ellipses) indeed captures the lack of correlation of perturbed abundances at time t_1+k and the strong correlation at time t_2+k ($k=3$). (b) (right) Community sensitivity decomposition at each point in time for the two-species model. Whereas community sensitivity (purple line) is dominated by the contribution of individual species (orange line) at time t_1 ($|\mathbf{P}| \approx 1$), it is dominated by the contribution of species correlations (green line) at time t_2 ($|\mathbf{P}| \ll 1$).

at \mathbf{N} and, therefore, can change along a trajectory (i.e., it is state-dependent). Also note that, in addition to knowing \mathbf{J} , knowledge of Σ_t and k is required to compute Σ . The accuracy of Σ in describing the distribution of perturbed abundances has been verified for communities at a stable fixed point (Arnoldi et al., 2018), whereas here we perform simulations to confirm this accuracy in other cases (Appendix S1: Section S2, Figure S1).

Without loss of generality, we can assume that $\mathbf{p}(t)$ and, therefore, $\mathbf{p}(t+k)$ follow a multivariate normal

distribution. In this case, the covariance matrices Σ_t and Σ can be visualized as 95% confidence S -dimensional ellipses surrounding perturbed abundances (Figure 2a). Importantly, the determinants $|\Sigma_t|$ and $|\Sigma|$ are proportional to the volume of such ellipses (Ives et al., 2003; Lu et al., 2021; Strang, 2016) and represent the overall change in species abundances following random pulse perturbations (i.e., community sensitivity). Alternatively, the change of an infinitesimal volume around \mathbf{N} (i.e., volume expansion rate) is given by the divergence

of the vector field \mathbf{f} : $\text{tr}(\mathbf{J}) = \sum_{i=1}^S \frac{\partial f_i}{\partial N_i} = \nabla \cdot \mathbf{f}(\mathbf{N})$ (Cenci & Saavedra, 2019; Strogatz, 2018). We show that $|\Sigma|$ is equivalent to $\text{tr}(\mathbf{J})$ via the following expression: $\log |\Sigma| = \log |\Sigma_t| + 2k\text{tr}(\mathbf{J})$ (*Materials and methods*). Thus, we define $\log |\Sigma|$ as our measure of state-dependent community sensitivity to perturbations and conclude that, for a fixed value of $|\Sigma_t|$ and k , a larger $\log |\Sigma|$ implies a larger $\text{tr}(\mathbf{J})$. Note that abundance changes must be interpreted in terms of their units and abundances are typically normalized when working with empirical data (*Materials and methods*).

Because the determinant of any covariance matrix can be written as the product of variances (σ_i^2) times the determinant of the correlation matrix \mathbf{P} (Appendix S1: Section S3), we can decompose the community sensitivity ($\log |\Sigma|$) into contributions of individual species and of species correlations:

$$\log |\Sigma| = \sum_{i=1}^S \log \sigma_i^2 + \log |\mathbf{P}|, \quad (1)$$

where the determinant of \mathbf{P} ($|\mathbf{P}|$) depends on all correlations ρ_{ij} between species i and j ($i, j = 1, \dots, S$). Note that ρ_{ij} is calculated by dividing the covariance between species i and j (i.e., i,j th element of Σ) by $\sigma_i \sigma_j$. Therefore, Equation (1) shows that species i impacts $\log |\Sigma|$ through its variance σ_i^2 (i.e., the sensitivity of species i to perturbations; Medeiros et al. [2023]), which expands the volume of perturbed abundances along a given direction (Figure 2a). In the absence of interspecific effects and correlations in initial perturbations (i.e., \mathbf{J} and Σ_t are diagonal matrices), $\mathbf{P} = \mathbf{I}$ and $|\mathbf{P}| = 1$, implying that $\log |\Sigma|$ is completely determined by $\sum_{i=1}^S \log \sigma_i^2$. However, in the presence of interspecific effects, $0 \leq |\mathbf{P}| \leq 1$, and species correlations impact community sensitivity by decreasing the volume of perturbed abundances (Figure 2a). That is, given a contribution of individual species ($\sum_{i=1}^S \log \sigma_i^2$), the contribution of species correlations ($\log |\mathbf{P}|$) can only decrease community sensitivity (i.e., decrease $\log |\Sigma|$) (Figure 2a). This result suggests that an intuitive way to understand the relative importance of species correlations is to consider the following ratio: $|\mathbf{P}| = \frac{|\Sigma|}{\prod_{i=1}^S \sigma_i^2}$.

Thus, $|\mathbf{P}| \rightarrow 1$ indicates that community sensitivity is completely explained by the contribution of individual species, whereas $|\mathbf{P}| \rightarrow 0$ indicates that community sensitivity is completely explained by the contribution of species correlations. This result is related to principal component analysis, where eigenvalues of the correlation matrix close to zero would indicate that the distribution of perturbed abundances is closer to an ellipse than to a circle (i.e., $|\mathbf{P}| \rightarrow 0$).

To illustrate how we can understand $\log |\Sigma|$ in light of $\sum_{i=1}^S \log \sigma_i^2$ and $\log |\mathbf{P}|$ (Figure 2b), we use again the

predator-prey model from Equation (2). As already shown in Figure 1, depending on the location of the community along this predator-prey cycle, species correlations will be weaker (Figure 1a,c) or stronger (Figure 1b,d). Figure 2b shows that Σ (black ellipses) indeed captures the changes in the distribution of perturbed abundances at time t_1 (weak species correlations) and time t_2 (strong species correlations). Importantly, this figure shows that depending on the community state (\mathbf{N}), $\log |\Sigma|$ (purple line) can be dominated by $\sum_{i=1}^S \log \sigma_i^2$ (orange line, t_1 , $|\mathbf{P}| \approx 1$) or by $\log |\mathbf{P}|$ (green line, t_2 , $|\mathbf{P}| \ll 1$; Figure 2b).

Understanding the contribution of species correlations using models

We now illustrate how our framework can provide important insights about the state-dependent impact of species correlations ($\log |\mathbf{P}|$) on community sensitivity to perturbations ($\log |\Sigma|$). To do so, we use three models that generate population dynamics without a stable fixed point: a two-species predator-prey model (Equation 2), a three-species food chain model (Equation 3), and a four-species competition model (Equation 4) (*Materials and methods*). We generate synthetic time series with 250 points ($\{\mathbf{N}(t)\}, t = 1, \dots, 250$) from each model and calculate the analytical Jacobian matrix evaluated at each $\mathbf{N}(t)$ (\mathbf{J} ; *Materials and methods*). Then, for each point in time, we compute the covariance matrix Σ and, finally, the contribution of species correlations as $\log |\mathbf{P}| = \log |\Sigma| - \sum_{i=1}^S \log \sigma_i^2$.

Figure 3 shows the contribution of species correlations ($\log |\mathbf{P}|$, green line) through time for each model. Overall, Figure 3 provides three main insights about the impact of species correlations on community sensitivity. First, for all models, we find a large variation in $\log |\mathbf{P}|$ over time. That is, there are points in time when species correlations have no impact on community sensitivity (i.e., $|\mathbf{P}| \approx 1$, for example, at time t_1) and points in time when they dominate community sensitivity (i.e., $|\mathbf{P}| \ll 1$, for example, at time t_4). Second, we find that \mathbf{P} (right panels in Figure 3) contains information that cannot be directly extracted from \mathbf{J} (left panels in Figure 3). Because we convert \mathbf{J} into Σ (and therefore into \mathbf{P}) by computing a matrix exponential (i.e., $e^{k\mathbf{J}}$), \mathbf{P} is the result of the sum of all indirect effects between species. Thus, the sign and strength of species correlations (ρ_{ij} ; for example right panel in Figure 3c) cannot be deduced from the sign and strength of interspecific effects (j_{ij} ; for example, left panel in Figure 3c). Finally, we find that, although $\log |\mathbf{P}|$ is a complicated nonlinear function of ρ_{ij} ($i, j = 1, \dots, S$) for large S , it is mainly driven by the strongest ρ_{ij} value in \mathbf{P} (e.g., right panel in Figure 3b and

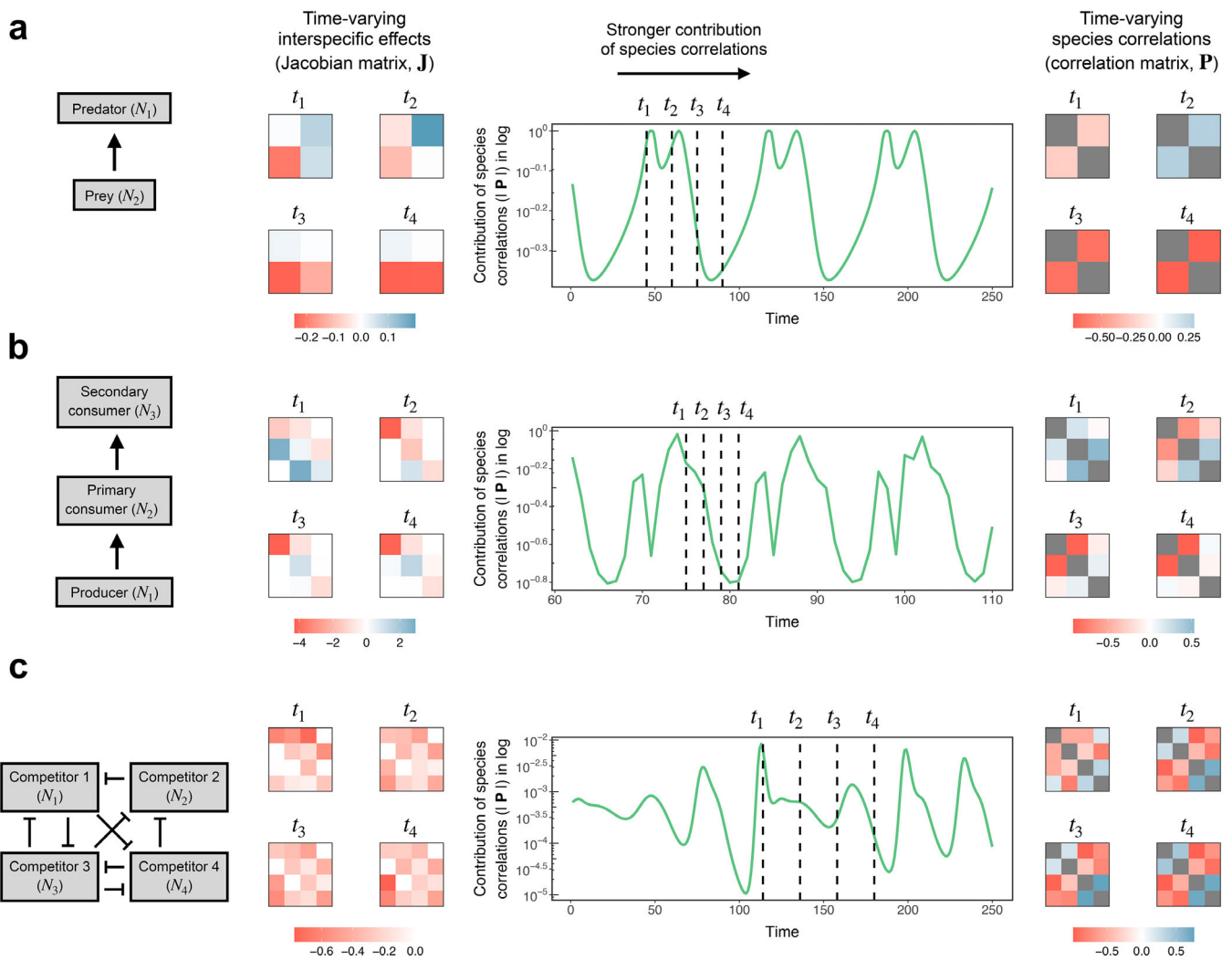


FIGURE 3 Impact of species correlated responses on community sensitivity changes over time under three population dynamics models. (a–c) (center) Contribution of species correlations to community sensitivity ($\log |\mathbf{P}|$, green line) over time for a two-species predator–prey model (a, Equation 2), a three-species food chain model (b, Equation 3), and a four-species competition model (c, Equation 4). Times t_1 through t_4 (vertical dashed lines) depict four arbitrary community states with an increasing contribution of species correlations (i.e., progressively lower $\log |\mathbf{P}|$). (a–c) (left) Jacobian matrix (\mathbf{J}) containing interspecific effects at each of the four states. (a–c) (right) Correlation matrix (\mathbf{P}) containing species correlated responses to perturbations at each of the four states. Although one or more correlation values in \mathbf{P} become stronger, there is no clear pattern in how \mathbf{J} changes from time t_1 to t_4 . Note that all diagonal elements in \mathbf{P} are equal to 1 and are colored in gray. Also note that we show a smaller time window for the three-species model to improve visualization.

Appendix S1: Figure S3). That is, higher values of $\max(\rho_{ij}^2)$ lead to more negative values of $\log |\mathbf{P}|$ (i.e., stronger contribution of species correlations; Appendix S1: Figure S3). We confirm this relationship between $\max(\rho_{ij}^2)$ and $\log |\mathbf{P}|$ by randomly generating multiple correlation matrices with up to $S=10$ species (Appendix S1: Figure S4). Because it is very likely that at least two species will respond in a correlated way in a large community (i.e., at least one large ρ_{ij}), this analysis also shows that $\log |\mathbf{P}|$ is expected to decrease with the number of species (Appendix S1: Figure S5).

Inferring the contribution of species correlations from time series

When dealing with empirical communities, there is typically a large uncertainty regarding model structure and parameters (Bartomeus et al., 2021; Cenci & Saavedra, 2019; Ye et al., 2015). Thus, calculating the time-varying Jacobian matrix (\mathbf{J}) using a parameterized model to investigate the impact of species correlations on community sensitivity can be unfeasible. In light of these limitations, we now show how to apply our framework by inferring \mathbf{J} directly from noisy time-series data without using model equations.

Given abundance time series for S species, we can infer \mathbf{J} at each point using a locally weighted state-space regression method known as the S-map (*Materials and methods*) (Cenci et al., 2019; Chang et al., 2021; Deyle et al., 2016; Sugihara, 1994). To verify the accuracy of inferring the contribution of species correlations ($\log |\mathbf{P}|$) from time series, we use the S-map to infer \mathbf{J} at each point in time for each of our three synthetic time series (*Materials and methods*). We then compute $\log |\mathbf{P}| = \log |\Sigma| - \sum_{i=1}^S \log \sigma_i^2$ at each point in time. We illustrate this entire procedure for the two-species predator-prey model in Appendix S1: Figure S7. Because empirical time series are usually contaminated with observational noise (Cenci et al., 2019; Sugihara, 1994), we apply Gaussian noise to each time series before performing the S-map (*Materials and methods*). Importantly, our framework focuses on inferring only two quantities: the trace of \mathbf{J} , which is equivalent to $\log |\Sigma|$, and the trace (in log) of Σ . By relying on an accurate inference of just these two quantities, our framework minimizes inference errors, especially in communities with a large number of species (Cenci et al., 2020; Cenci & Saavedra, 2019). Note, however, that the amount of time-series data required to accurately infer the Jacobian matrix grows exponentially with the number of species (Cenci et al., 2019; Chang et al., 2021).

Because we can only infer the elements of \mathbf{J} up to a constant (Cenci & Saavedra, 2019) and the value of $\log |\mathbf{P}|$ depends on S and k (Appendix S1: Figures S5 and S6), here we focus on qualitatively detecting points in time with extreme (low or high) values of $\log |\mathbf{P}|$ (*Materials and methods*). We find the inferred $\log |\mathbf{P}|$ to be very similar over time to the analytical $\log |\mathbf{P}|$ for all three synthetic time series (Figure 4). In particular, for all synthetic time series, we obtain an accuracy approximately twice as high as the 25% accuracy of a random guess: 43.6% for the two-species predator-prey model (Figure 4a), 54.8% for the three-species food chain model (Figure 4b), and 53.2% for the four-species competition model (Figure 4c). Note that if we were randomly classifying points as having a low or high $\log |\mathbf{P}|$ (instead of using the inferred $\log |\mathbf{P}|$), our accuracy of matching the analytical classification would be, on average, 25%. Although our accuracy can decrease with stronger observational noise and under uncertainty in Σ_t and k (*Materials and methods*), we still obtain an accuracy higher than 25% for most cases (Appendix S1: Figures S8 and S9).

Most importantly, we find low and high values of $\log |\mathbf{P}|$ to be concentrated along certain regions of each attractor (Figure 4 and Appendix S1: Figure S11). For example, for the two-species predator-prey model, we find that species correlations can only decrease

community sensitivity when the prey abundance (N_2) is high (Figure 4a). We confirm this result with an additional two-species predator-prey model (Appendix S1: Figure S11) and find similar simple state dependencies in the three-species food chain model (Figure 4b) and in the four-species competition model (Figure 4c). These results suggest that the impact of species correlations should only be observed under certain species abundance states, which we can accurately detect using an inference approach based on time-series data.

Application to experimental communities

Lastly, we showcase our framework using two empirical communities to gain further insights into how and when species correlations may reduce community sensitivity to perturbations. We use two experimental time series with two and three species that have been shown to exhibit cyclic and chaotic dynamics, respectively, under laboratory conditions (Becks et al., 2005; Blasius et al., 2020) (*Materials and methods*). Following our analyses with synthetic time series, we apply the S-map to both time series to infer the contribution of species correlations to community sensitivity over time as $\log |\mathbf{P}| = \log |\Sigma| - \sum_{i=1}^S \log \sigma_i^2$. Given our accuracy in detecting regions with extreme (low or high) values of $\log |\mathbf{P}|$ in synthetic time series (Figure 4), we follow the same procedure for these experimental time series.

We find that the ratio between community sensitivity and the contribution of individual species $\left(|\mathbf{P}| = \frac{|\Sigma|}{\prod_{i=1}^S \sigma_i^2}\right)$ changes considerably across time for both the two-species (range of $|\mathbf{P}|$: 0.77–0.99, Figure 5a) and the three-species community (range of $|\mathbf{P}|$: 0.64–0.93, Figure 5b). Note that $|\mathbf{P}|$ depends on time step k and can decrease (i.e., contribution of species correlations can increase) when this time step is larger (Appendix S1: Figure S12). This suggests that the contribution of either individual species or species correlations can dominate the sensitivity of these communities ($|\mathbf{P}|$ close to 1 or close to 0, respectively), depending on the point in time. In fact, as expected from our analyses with synthetic time series, we find that time-series points with low or high $\log |\mathbf{P}|$ (dark or light green points in Figure 5a,b) are clearly separated in the state space of species abundances. For the two-species community, we find that prey abundance is high when the contribution of species correlations is high and prey abundance is low when this contribution is low (two-sample t -test: $t(118.7) = 10.02$, $p < 0.0001$). Thus, we find a similar state-dependent pattern in $\log |\mathbf{P}|$ in the two-species experimental community (Figure 5a) and

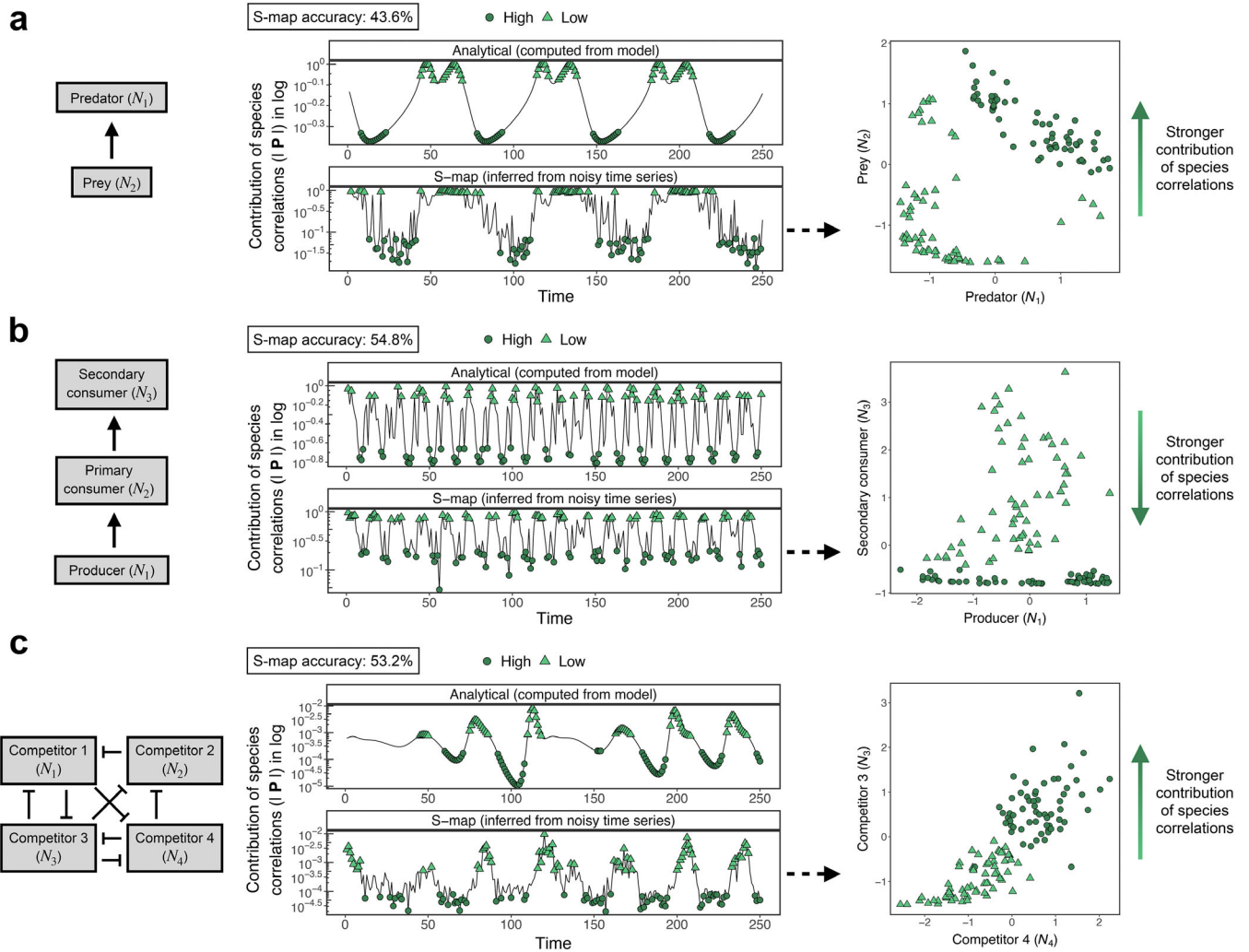


FIGURE 4 State-dependent impact of species correlated responses can be inferred directly from noisy time series. (a–c) (center) For each population dynamics model (a, Equation 2; b, Equation 3; c, Equation 4), the top panel shows the contribution of species correlations ($\log |\mathbf{P}|$) over time computed analytically from the model equations, whereas the bottom panel shows $\log |\mathbf{P}|$ inferred from the noisy time series with the S-map. Values of $\log |\mathbf{P}|$ for each panel are independently classified as having a high (dark green circles) or low (light green triangles) contribution to community sensitivity. Points not classified as high or low are not shown to improve visualization. The S-map accuracy indicates the percentage of high and low points in the bottom panel that match those in the top panel (expected accuracy of random guess: 25%). (a–c) (right) State space of species abundances (with noise and normalized) for each model showing that the inferred high and low values of $\log |\mathbf{P}|$ are concentrated along certain community states. For instance, species correlations only reduce community sensitivity when the prey abundance is high under the two-species model (a). Note that for the three- and four-species models (b, c) we show the two species that most clearly separate high and low values of $\log |\mathbf{P}|$.

in the two-species predator-prey model (Figure 4a and Appendix S1: Figure S11). Interestingly, we also find that time windows with coherent predator-prey cycles (Blasius et al., 2020) retain this strong state-dependent pattern, whereas time windows with noncoherent cycles do not show the state-dependent pattern (Appendix S1: Figure S10). As for the three-species community, we find that the abundance of the preferred prey is low when the contribution of species correlations is high and the abundance of the preferred prey is high when this contribution is low (two-sample

t-test: $t(9.69) = -3.38$, $p = 0.007$). This result provides further evidence that the impact of species correlations on community sensitivity depends on the abundance of particular species.

DISCUSSION

The response of an ecological community to perturbations (e.g., recovery, constancy, sensitivity) is a property that emerges from the responses of its constituent species

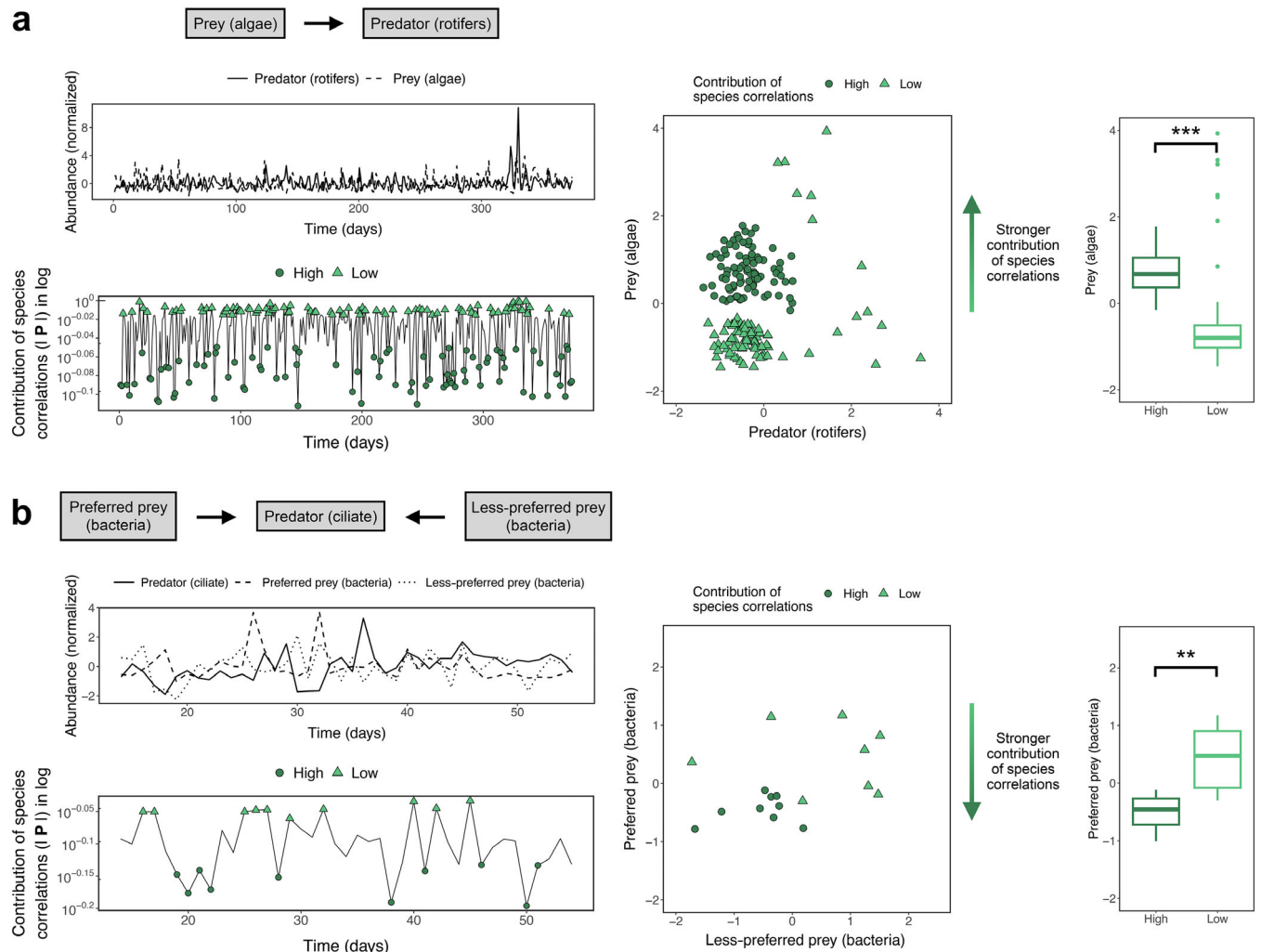


FIGURE 5 Impact of species correlated responses depends on prey abundance for two experimental communities. (a) (left) The top panel shows the (normalized) abundance time series of a predator (rotifers, solid line) and its prey (algae, dashed line; data from Blasius et al. [2020]). The bottom panel shows the contribution of species correlations to community sensitivity ($\log |P|$) with points being classified as having a high (dark green circles) or low (light green triangles) contribution. Points not classified as high or low are not shown to improve visualization. (a) (right) The left panel shows the state space of species abundances with each point colored according to the contribution of species correlations. The right panel shows that the prey abundance (boxplots) is higher for points with a high than with a low contribution (asterisks denote $p < 0.0001$ for a two-sample t -test). (b) (left) The top panel shows the (normalized) abundance time series of a predator (ciliate, solid line), its preferred prey (bacteria, dashed line), and its less-preferred prey (bacteria, dotted line; data from Becks et al. [2005]). The bottom panel shows $\log |P|$ over time with points being classified as in (a). (b) (right) The left panel shows the state space of prey abundances with each point colored according to the contribution of species correlations. The right panel shows that the preferred prey abundance (boxplots) is lower for points with a high than with a low contribution (asterisks denote $p = 0.007$ for a two-sample t -test).

and the interactions among them (Kéfi et al., 2019; Pennekamp et al., 2018; Pimm, 1984; Tilman et al., 2006). Hence, understanding how responses at the species-level scale up to shape the response of the whole community has remained an important problem in ecology (Clark et al., 2021; Kéfi et al., 2019; Levin & Lubchenco, 2008; White et al., 2020). In this study, we tackled this problem when population dynamics fluctuate and, therefore, interspecific effects (i.e., elements of the Jacobian matrix) change over time and have time-varying impacts on whole-community response to perturbations. Our work

provides three main insights into how species correlated responses to perturbations impact whole-community response.

First, by developing a framework to decompose the community sensitivity to perturbations into contributions of individual species and of species correlations, we demonstrate that correlations (positive or negative) can only dampen community sensitivity (Figure 2). Previous work on compensatory dynamics established that negative correlations increased the constancy of total abundance, whereas positive correlations decreased it (Brown et al.,

2016; Fischer et al., 2001; Gonzalez & Loreau, 2009; Tilman et al., 2006). Although constancy is an important measure of community response, it can only be computed over a long stretch of time (i.e., is not state-dependent) and is most relevant when abundances are assumed to be at a stable fixed point (Gonzalez & Loreau, 2009). Under the abundance fluctuations investigated here, the volume expansion rate of perturbed abundances (Cenci et al., 2020; Cenci & Saavedra, 2019; Ives et al., 2003) provides a more meaningful and state-dependent measure of the short-term community response to perturbations. Overall, based on our framework, there are two ways for perturbed abundances to have a small volume expansion rate in state space: The contribution of individual species is low (i.e., variances in Σ are small) or the contribution of species correlations is high (i.e., $|\mathbf{P}|$ is close to zero). Note that if variances in Σ are large but $|\mathbf{P}|$ is close to zero, perturbed abundances will stretch along one or more directions in state space even if the volume expansion rate is small. Thus, a small volume expansion rate must be carefully interpreted in large communities for which perturbed abundances can still stretch along certain directions. Overall, to understand how perturbations might affect an entire community (Cenci & Saavedra, 2019), it is important to combine information on the response of individual species (Medeiros et al., 2023) with information on species correlations.

Second, we find that the impact of species correlations on community sensitivity changes over time and essentially depends on the maximum squared correlation value in the correlation matrix \mathbf{P} (Figure 3). Thus, a single strong correlation value in \mathbf{P} (positive or negative) is generally sufficient to bring $|\mathbf{P}|$ close to zero, greatly reducing the volume expansion rate (i.e., reducing community sensitivity). This single strong correlation provides a simple mechanism for how a pair of species responding together to perturbations may dampen community sensitivity, although this mechanism may not be enough in large communities (Appendix S1: Figure S4). In addition, we show that the covariance matrix Σ results from a sum of all indirect effects between species (Equation 6), suggesting a nontrivial relationship between interspecific effects and species correlations. Given the importance of indirect effects for ecological dynamics in species-rich communities (Pires et al., 2020; Saavedra et al., 2017; Wootton, 1994), investigating the links between time-varying interspecific effects and species correlations could be an interesting future direction. Specifically, combining our framework with recent improvements of the S-map approach to inferring the Jacobian matrix of large communities from time series can be a fruitful research avenue (Cenci et al., 2019; Chang et al., 2021).

Finally, we find that the contribution of species correlations to community sensitivity depends on community state under both models (Figure 4) and data (Figure 5). That is, even though population dynamics may follow a cyclic or chaotic attractor (i.e., perturbed abundances eventually return to the attractor), short-term responses to perturbations may vary considerably along the attractor. In particular, points in time with a high or low contribution of species correlations are not scattered along a cyclic or chaotic attractor but, rather, are confined to specific regions of the state space of abundances. Therefore, our results indicate that species correlations may only contribute to decrease community sensitivity under certain values of species abundances (e.g., when prey abundance is high; Figures 4a and 5a). Previous food web studies found that species responses after predator removal or introduction depended on the sign and strength of species interactions (Samhouri et al., 2017; Schneider et al., 2012; Worsfold et al., 2009). We find an extension of these results for cases where state-dependent interspecific effects create state-dependent species correlations. Given that consumer-resource interactions frequently generate cyclic or chaotic dynamics (Becks et al., 2005; Begon et al., 1996; Blasius et al., 2020; Deyle et al., 2016; Hastings & Powell, 1991), such state-dependent impacts of species correlations on community response to perturbations may be widespread in natural communities. Here, we focus on small communities under controlled conditions as the best-case scenario to verify whether the patterns that we observe under models also appear in the data. Nevertheless, applying our framework to natural communities should be an interesting next step if a long time series depicting an attractor is available. A final caveat is that our framework does not address other realistic cases where communities undergo nonequilibrium transient dynamics, a challenge that remains for future research.

A potential application of these state-dependent patterns is that, in regions with strong correlated responses, an intentional perturbation on a given species should inform us about the response of another species (e.g., Figure 1a,b). This could be useful, for instance, if we wish to add or remove individuals of a given species but want some other species to change as little as possible (e.g., blue trajectory in Figure 1b). Thus, by decreasing whole-community sensitivity to perturbations, species correlations increase the predictability of perturbation outcomes. All in all, our framework allows us to better understand how and when species interactions can dampen community sensitivity to perturbations when we relax the assumption that communities are at a stable fixed point.

MATERIALS AND METHODS

Synthetic time series from population dynamics models

We use three synthetic time series generated from population dynamics models with $S=2$, $S=3$, and $S=4$ species to illustrate the impact of species correlations on community sensitivity to perturbations. The first model depicts the population dynamics of a predator (Species 1) and its prey (Species 2) (Yodzis, 1989):

$$\begin{aligned}\frac{dN_1}{dt} &= cN_1 \left(\frac{aN_2^2}{1 + ahN_2^2} \right) - dN_1, \\ \frac{dN_2}{dt} &= rN_2 \left(1 - \frac{N_2}{K} \right) - N_1 \left(\frac{aN_2^2}{1 + ahN_2^2} \right),\end{aligned}\quad (2)$$

where c and d are the predator conversion and death rates, a is the encounter rate, h is the handling time, and r and K are the prey intrinsic growth rate and carrying capacity, respectively. Here, we explore the limit cycle that emerges when $c=0.5$, $a=0.002$, $h=4$, $d=0.1$, $r=0.5$, and $K=100$ (Yodzis, 1989) (Figure 1 and Appendix S1: Figure S2). The second model depicts a food chain with a producer (Species 1), a primary consumer (Species 2), and a secondary consumer (Species 3) (Hastings & Powell, 1991):

$$\begin{aligned}\frac{dN_1}{dt} &= rN_1 \left(1 - \frac{N_1}{K} \right) - \frac{a_1 N_1 N_2}{1 + b_1 N_1}, \\ \frac{dN_2}{dt} &= -sN_2 + hN_1 N_2 - \frac{a_2 N_2 N_3}{1 + b_2 N_2}, \\ \frac{dN_3}{dt} &= -lN_3 + nN_2 N_3,\end{aligned}\quad (3)$$

where r and K are the producer intrinsic growth rate and carrying capacity, a_1 and a_2 are encounter rates, b_1 and b_2 are handling times, s and l are consumer death rates, and h and n are consumer conversion rates. We explore the chaotic attractor that arises when $r=4.3$, $K=50$, $a_1=0.1$, $b_1=0.1$, $a_2=0.1$, $b_2=0.1$, $s=1$, $h=0.05$, $l=1$, and $n=0.03$ (Upadhyay, 2000) (Appendix S1: Figure S2). The third model consists of the classic Lotka–Volterra model with competitive interactions (Case, 2000):

$$\frac{dN_i}{dt} = N_i \left(r_i + \sum_{j=1}^S a_{ij} N_j \right), \quad (4)$$

where r_i ($r_i > 0$) is an element of the vector \mathbf{r} representing the intrinsic growth rate of species i , and a_{ij} ($a_{ij} \leq 0$) is an element of the interaction matrix \mathbf{A} representing the per-capita effect of species j on species i . We investigate

the chaotic attractor that emerges with $S=4$ and the following parameter values (Vano et al., 2006) (Appendix S1: Figure S2):

$$\mathbf{r} = \begin{bmatrix} 1 \\ 0.72 \\ 1.53 \\ 1.27 \end{bmatrix}, \quad \mathbf{A} = \begin{bmatrix} -1 & -1.09 & -1.52 & 0 \\ 0 & -1 & -0.44 & -1.36 \\ -2.33 & 0 & -1 & -0.47 \\ -1.21 & -0.51 & -0.35 & -1 \end{bmatrix}.$$

For each model, we first numerically integrate the dynamics using a Runge–Kutta method with a time step of 0.05 and obtain a time series with 5000 points. Then we sample equidistant points, obtaining a final multivariate time series with 250 points ($\{\mathbf{N}(t)\}$, $t=1, \dots, 250$). Using this protocol, we obtain time series that fully sample the attractor of each model (Appendix S1: Figure S2).

Community sensitivity as volume expansion rate

A generic population dynamics model for a community with S species may be written $\frac{d\mathbf{N}}{dt} = \mathbf{f}(\mathbf{N})$, where $\mathbf{N} = [N_1, \dots, N_S]^\top$ is the vector of species abundances and $\mathbf{f} = (f_1, \dots, f_S)$ ($f_i: \mathbb{R}^S \rightarrow \mathbb{R}$) is a set of functions. At any given state \mathbf{N} , this community can be affected by a small pulse perturbation $\mathbf{p} = [p_1, \dots, p_S]^\top$ that changes \mathbf{N} into $\tilde{\mathbf{N}}$ (Bender et al., 1984). The linearized dynamics of such a perturbation is given by (Appendix S1: Section S1) (Medeiros et al., 2023; Strogatz, 2018)

$$\frac{d\mathbf{p}}{dt} = \mathbf{J} \Big|_{\tilde{\mathbf{N}}=\mathbf{N}} \cdot \mathbf{p}, \quad (5)$$

where $\mathbf{J}|_{\tilde{\mathbf{N}}=\mathbf{N}}$ (hereafter \mathbf{J}) is the Jacobian matrix of partial derivatives with elements $j_{ij} = \frac{\partial f_i}{\partial N_j}$ (interspecific effects) evaluated at \mathbf{N} . Note that \mathbf{J} is state-dependent as it depends on the community state \mathbf{N} . We assume that perturbations at an arbitrary time t ($\mathbf{p}(t)$) follow a distribution with mean vector μ_t and covariance matrix Σ_t (Figure 2a). Although this is not necessary for our derivation (Appendix S1: Section S1), we focus on perturbations that are not biased in a given direction (i.e., $\mu_t = \mathbf{0}$) and that affect each species equally and independently (i.e., $\Sigma_t = c\mathbf{I}$, where \mathbf{I} is the identity matrix and c is the perturbation variance). After k time steps, the covariance matrix describing the distribution of $\mathbf{p}(t+k)$ will be given by (Appendix S1: Section S1) (Arnoldi et al., 2018; Medeiros et al., 2023)

$$\Sigma = e^{k\mathbf{J}} \Sigma_t e^{k\mathbf{J}^\top}, \quad (6)$$

where $e^{\mathbf{A}} = \sum_{i=1}^{\infty} \frac{1}{i!} \mathbf{A}^i$ is the exponential of matrix \mathbf{A} .

Because the determinant of a matrix represents the volume of the S -dimensional parallelepiped formed by its row vectors (Lu et al., 2021; Strang, 2016), the volume of perturbed abundances at times t and $t+k$ will be proportional to the determinants of the respective covariance matrices: $|\Sigma_t|$ and $|\Sigma|$. Here, we are interested in the change in volume from time t to $t+k$ and, therefore, consider the volume of initial perturbations ($|\Sigma_t|$) to be fixed. The determinant of Σ is then given by

$$\begin{aligned} |\Sigma| &= |e^{k\mathbf{J}} \Sigma_t e^{k\mathbf{J}^T}| \\ &= |\Sigma_t| |e^{k\mathbf{J}} e^{k\mathbf{J}^T}| \\ &= |\Sigma_t| |e^{2k\Lambda}| \\ &= |\Sigma_t| \prod_{i=1}^S e^{2k\lambda_i}, \end{aligned} \quad (7)$$

where Λ is a diagonal matrix containing the eigenvalues of $\mathbf{J}(\lambda_1, \dots, \lambda_S)$. Taking the logarithm of both sides of Equation (7), we obtain a connection to the volume expansion rate:

$$\begin{aligned} \log |\Sigma| &= \log \left(|\Sigma_t| \prod_{i=1}^S e^{2k\lambda_i} \right) \\ &= \log |\Sigma_t| + 2k \sum_{i=1}^S \lambda_i \\ &= \log |\Sigma_t| + 2k \text{tr}(\mathbf{J}), \end{aligned} \quad (8)$$

where $\text{tr}(\mathbf{J})$ is the trace of \mathbf{J} . Note that $\text{tr}(\mathbf{J}) = \sum_{i=1}^S \frac{\partial f_i}{\partial N_i} = \nabla \cdot \mathbf{f}(\mathbf{N})$ represents the divergence of the vector field \mathbf{f} around \mathbf{N} (i.e., volume expansion rate) (Cenci et al., 2020; Cenci & Saavedra, 2019; Strogatz, 2018). Therefore, $\log |\Sigma|$ is equivalent to $\text{tr}(\mathbf{J})$ and represents the community sensitivity to pulse perturbations on abundances.

Computing the contribution of species correlations from time series

For each synthetic time series generated from a population dynamics model, we compute the time-varying contribution of species correlations ($\log |\mathbf{P}|$) in two different ways. Recall that $\log |\mathbf{P}|$ is given by the difference between the community sensitivity ($\log |\Sigma|$) and the contribution of individual species ($\sum_{i=1}^S \log \sigma_i^2$) (Equation 1). First, we compute $\log |\mathbf{P}|$ analytically by calculating \mathbf{J} from the model equations (Equations 2–4) and evaluating it at each $\mathbf{N}(t)$. Second, we compute $\log |\mathbf{P}|$ by inferring \mathbf{J} directly from the time series with the S-map method (see next section). To compute Σ , we assume minimal

knowledge of the distribution and evolution of perturbations and set $\Sigma_t = \mathbf{I}$ and k at a fixed value over time ($k=3$ for two-species predator-prey and four-species competition models, and $k=0.5$ for the three-species food chain model). These values of k are proportional to the average rate of change (i.e., $\frac{d\mathbf{N}}{dt}$) of each model and using other values of k gives qualitatively similar results (Appendix S1: Figure S6). Then, for each point in time, we use Σ to calculate the contribution of species correlations as $\log |\mathbf{P}| = \log |\Sigma| - \sum_{i=1}^S \log \sigma_i^2$.

Instead of focusing on the exact values of $\log |\mathbf{P}|$ over time, here we focus on qualitatively detecting community states with extreme (low or high) $\log |\mathbf{P}|$ values. That is, after computing $\log |\mathbf{P}|$ analytically (hereafter analytical $\log |\mathbf{P}|$) or with the S-map (hereafter inferred $\log |\mathbf{P}|$), we classify each time-series point as having a low (i.e., $\log |\mathbf{P}|$ higher than its 75th percentile) or high (i.e., $\log |\mathbf{P}|$ lower than its 25th percentile) contribution of species correlations. We perform this classification independently for the analytical and inferred $\log |\mathbf{P}|$. Then, to test the accuracy of inferring $\log |\mathbf{P}|$ with the S-map, for each synthetic time series, we compute the percentage of points classified as having a low (or high) analytical $\log |\mathbf{P}|$ that also have a low (or high) inferred $\log |\mathbf{P}|$. Note that the random expectation of this accuracy (e.g., if we shuffled the inferred $\log |\mathbf{P}|$ values) is 25%.

Inferring the time-varying Jacobian matrix with the S-map

Here we describe the S-map, a locally weighted state-space regression method that has been shown to provide accurate inferences of the time-varying Jacobian matrix (\mathbf{J}) from time series (Appendix S1: Figure S7) (Cenci et al., 2019; Chang et al., 2021; Deyle et al., 2016; Sugihara, 1994). Given a multivariate time series containing the abundances of S species over T time points ($\{\mathbf{N}(t)\}$, $t=1, \dots, T$), the S-map allows us to infer \mathbf{J} at each point. This method is based on fitting a linear regression of the following form to the time series: $N_i(t+1) = c_{i0} + \sum_{j=1}^S c_{ij} N_j(t)$, where $c_{ij} = \frac{\partial N_i(t+1)}{\partial N_j(t)}$ is a discrete-time approximation of the Jacobian matrix element j_{ij} . However, fitting this linear regression would not capture the state-dependent nature of \mathbf{J} , that is, \mathbf{J} fundamentally depends on \mathbf{N} . Thus, the S-map consists of fitting this linear regression locally for each target point $\mathbf{N}(t^*)$ by giving a stronger weight to points that are closer to it in state space. This is done by finding a solution for \mathbf{c} in $\mathbf{b} = \mathbf{Ac}$, where $b_t = w_t N_i(t+1)$, $a_{tj} = w_t N_j(t)$, $w_t = \exp \left[-\theta \frac{\|\mathbf{N}(t) - \mathbf{N}(t^*)\|}{\bar{d}} \right]$, and $\bar{d} = \frac{1}{T} \sum_{t=1}^T \|\mathbf{N}(t) - \mathbf{N}(t^*)\|$.

Thus, $\mathbf{b} \in \mathbb{R}^{T-1}$ contains the abundances at $t+1$ weighted by the relative distance of each point to the target point, $\mathbf{A} \in \mathbb{R}^{(T-1) \times (S+1)}$ is the weighted data matrix of abundances at t , and $\mathbf{c} \in \mathbb{R}^{S+1}$ estimates the i th row of \mathbf{J} at $\mathbf{N}(t^*)$ as well as an intercept term. We obtain the solution for \mathbf{c} via singular value decomposition (Deyle et al., 2016), which is equivalent to the ordinary least-squares solution (Cenci et al., 2019). Finally, the parameter θ determines how strongly the regression is localized around each target point $\mathbf{N}(t^*)$, and we select its value via abundance predictions with leave-one-out cross-validation (Cenci et al., 2019). That is, for a given θ value, we fit the S-map to the time series after removing one of its points (e.g., $\mathbf{N}(t')$), use \mathbf{J} at $\mathbf{N}(t'-1)$ to predict $\mathbf{N}(t')$, and repeat this procedure by removing each of the T points. We then select the θ value that minimizes the mean prediction error across all T abundance predictions.

We use the S-map on the three synthetic time series to test the accuracy of this method in inferring the time-varying contribution of species correlations ($\log |\mathbf{P}|$). To do so, we first apply Gaussian noise to each synthetic time series. Specifically, for each species i and time t , we transform $N_i(t)$ into $N_i(t) + N(\mu=0, \sigma^2 = [\delta N_i(t)]^2)$, where $\delta = 0.1$ (see Appendix S1: Figure S8 for $\delta = 0.2$). Then, for each time series, we fit the S-map with the leave-one-out cross-validation procedure to select the best θ parameter and use this value of θ to fit the S-map to the whole time series and obtain \mathbf{J} at each point in time. Because species abundances typically vary in scale, we normalize each noisy time series to zero mean and unit standard deviation prior to apply the S-map (Cenci et al., 2019; Deyle et al., 2016; Ushio et al., 2018). Following the analysis with the analytical matrix \mathbf{J} (see previous section), we use each inferred matrix \mathbf{J} to compute Σ by setting $\Sigma_t = \mathbf{I}$ and k to be a fixed value over time. We also perform these analyses by adding noise to Σ_t and k to test the robustness of our framework to uncertainty in these quantities (Appendix S1: Figure S9).

Inferring the contribution of species correlations in experimental communities

Here we describe how we apply our framework to two experimental time series. The first time series represents a two-species microcosm community containing the rotifer *Brachionus calyciflorus* as a predator species and the alga *Monoraphidium minutum* as its prey species (Blasius et al., 2020). This community has been shown to exhibit population cycles under constant experimental conditions for approximately 300 predator generations (Blasius et al., 2020). Due to eight missing data points and small differences in sampling intervals, we interpolate the original

time series using cubic hermite interpolation to obtain a final time series with 358 points and equidistant sampling intervals of 1.045 days. Using the original time series gave very similar results to what is shown in Figure 5a. Because this time series contains windows with coherent and noncoherent predator-prey cycles (Blasius et al., 2020), we also performed our analyses using one window with mostly coherent and one window with mostly noncoherent cycles, both with 80 points (Appendix S1: Figure S10).

The second time series represents a three-species chemostat community containing the ciliate *Tetrahymena pyriformis* as a predator species and the bacteria *Pedobacter* sp. and *Brevundimonas* sp. as its two prey species (Becks et al., 2005; Pennekamp et al., 2019). It has been demonstrated that under some experimental conditions, this community can exhibit chaotic dynamics (i.e., positive Lyapunov exponent) (Becks et al., 2005). Because this time series contains equal sampling intervals of 1 day, we did not use an interpolation procedure for it. We use the time series starting from Day 14 because of several missing data points prior to this day, which resulted in a final time series with 42 points. Note that 42 points are more than enough to apply the S-map to a three-species community (Munch et al., 2020).

After the previously described time series treatment, we apply the S-map (see previous section) to both time series to infer $\log |\mathbf{P}|$ over time. Because of scale differences in species abundances, we normalize each time series to zero mean and unit SD before applying the S-map. Following our analyses with synthetic time series, we select θ with leave-one-out cross-validation (see previous section) and use the selected value to fit the S-map to the whole time series and compute $\log |\mathbf{P}| = \log |\Sigma| - \sum_{i=1}^S \log \sigma_i^2$ at each point in time. We use each inferred matrix \mathbf{J} to compute Σ by setting $\Sigma_t = \mathbf{I}$ and $k = 1$ because we have no information about how perturbations could impact these communities (see Appendix S1: Figure S12 for $k = 3$). Finally, we classify each time series point as showing a low (i.e., $\log |\mathbf{P}|$ higher than its 75th percentile) or high (i.e., $\log |\mathbf{P}|$ lower than its 25th percentile) contribution of species correlations.

AUTHOR CONTRIBUTIONS

Lucas P. Medeiros and Serguei Saavedra designed the research. Lucas P. Medeiros performed the analyses. Serguei Saavedra supervised the study. Lucas P. Medeiros wrote the paper, and Serguei Saavedra contributed to revisions.

ACKNOWLEDGMENTS

We thank C. Long, J. Deng, C. Song, V. Dakos, G. Sugihara, T. Lieberman, and D. Rothman for insightful discussions and suggestions regarding this work.

Lucas P. Medeiros was supported by the Massachusetts Institute of Technology (MIT) Environmental Solutions Initiative and the Martin Family Society of Fellows for Sustainability. Serguei Saavedra was supported by the National Science Foundation DEB-2024349 and the MIT Sea Grant Program.

CONFLICT OF INTEREST STATEMENT

The authors declare no conflicts of interest.

DATA AVAILABILITY STATEMENT

Data and R code supporting the results are archived on Zenodo: <https://doi.org/10.5281/zenodo.7968611> (Medeiros & Saavedra, 2023).

ORCID

Lucas P. Medeiros  <https://orcid.org/0000-0002-0320-5058>

Serguei Saavedra  <https://orcid.org/0000-0003-1768-363X>

REFERENCES

- Arnoldi, J.-F., A. Bideault, M. Loreau, and B. Haegeman. 2018. "How Ecosystems Recover from Pulse Perturbations: A Theory of Short-to Long-Term Responses." *Journal of Theoretical Biology* 436: 79–92.
- Bartomeus, I., S. Saavedra, R. P. Rohr, and O. Godoy. 2021. "Experimental Evidence of the Importance of Multitrophic Structure for Species Persistence." *Proceedings of the National Academy of Sciences* 118: e2023872118.
- Becks, L., F. M. Hilker, H. Malchow, K. Jürgens, and H. Arndt. 2005. "Experimental Demonstration of Chaos in a Microbial Food Web." *Nature* 435: 1226–9.
- Begon, M., S. M. Sait, and D. J. Thompson. 1996. "Predator–Prey Cycles with Period Shifts between Two-and Three-Species Systems." *Nature* 381: 311–5.
- Bender, E. A., T. J. Case, and M. E. Gilpin. 1984. "Perturbation Experiments in Community Ecology: Theory and Practice." *Ecology* 65: 1–13.
- Blasius, B., L. Rudolf, G. Weithoff, U. Gaedke, and G. F. Fussmann. 2020. "Long-Term Cyclic Persistence in an Experimental Predator–Prey System." *Nature* 577: 226–30.
- Brown, B. L., A. L. Downing, and M. A. Leibold. 2016. "Compensatory Dynamics Stabilize Aggregate Community Properties in Response to Multiple Types of Perturbations." *Ecology* 97: 2021–33.
- Cardinale, B. J., J. E. Duffy, A. Gonzalez, D. U. Hooper, C. Perrings, P. Venail, A. Narwani, et al. 2012. "Biodiversity Loss and its Impact on Humanity." *Nature* 486: 59–67.
- Carpenter, S. R., N. F. Caraco, D. L. Correll, R. W. Howarth, A. N. Sharpley, and V. H. Smith. 1998. "Nonpoint Pollution of Surface Waters with Phosphorus and Nitrogen." *Ecological Applications* 8: 559–68.
- Case, T. 2000. *An Illustrated Guide to Theoretical Ecology*. Oxford: Oxford University Press.
- Cenci, S., L. P. Medeiros, G. Sugihara, and S. Saavedra. 2020. "Assessing the Predictability of Nonlinear Dynamics under Smooth Parameter Changes." *Journal of the Royal Society Interface* 17: 20190627.
- Cenci, S., and S. Saavedra. 2019. "Non-parametric Estimation of the Structural Stability of Non-equilibrium Community Dynamics." *Nature Ecology & Evolution* 3: 912–8.
- Cenci, S., G. Sugihara, and S. Saavedra. 2019. "Regularized s-Map for Inference and Forecasting with Noisy Ecological Time Series." *Methods in Ecology and Evolution* 10: 650–60.
- Chang, C.-W., T. Miki, M. Ushio, P.-J. Ke, H.-P. Lu, F.-K. Shiah, and C.-H. Hsieh. 2021. "Reconstructing Large Interaction Networks from Empirical Time Series Data." *Ecology Letters* 24: 2763–74.
- Clark, A. T., J.-F. Arnoldi, Y. R. Zelnik, G. Barabas, D. Hodapp, C. Karakoç, S. König, et al. 2021. "General Statistical Scaling Laws for Stability in Ecological Systems." *Ecology Letters* 24: 1474–86.
- Cochrane, M. A. 2003. "Fire Science for Rainforests." *Nature* 421: 913–9.
- Deyle, E. R., R. M. May, S. B. Munch, and G. Sugihara. 2016. "Tracking and Forecasting Ecosystem Interactions in Real Time." *Proceedings of the Royal Society B: Biological Sciences* 283: 20152258.
- Dulvy, N. K., J. D. Metcalfe, J. Glanville, M. G. Pawson, and J. D. Reynolds. 2000. "Fishery Stability, Local Extinctions, and Shifts in Community Structure in Skates." *Conservation Biology* 14: 283–93.
- Estes, J. A., M. T. Tinker, T. M. Williams, and D. F. Doak. 1998. "Killer Whale Predation on Sea Otters Linking Oceanic and Nearshore Ecosystems." *Science* 282: 473–6.
- Fischer, J. M., T. M. Frost, and A. R. Ives. 2001. "Compensatory Dynamics in Zooplankton Community Responses to Acidification: Measurement and Mechanisms." *Ecological Applications* 11: 1060–72.
- Gonzalez, A., and M. Loreau. 2009. "The Causes and Consequences of Compensatory Dynamics in Ecological Communities." *Annual Review of Ecology, Evolution, and Systematics* 40: 393–414.
- Hastings, A., K. C. Abbott, K. Cuddington, T. Francis, G. Gellner, Y.-C. Lai, A. Morozov, S. Petrovskii, K. Scranton, and M. L. Zeeman. 2018. "Transient Phenomena in Ecology." *Science* 361: eaat6412.
- Hastings, A., and T. Powell. 1991. "Chaos in a Three-Species Food Chain." *Ecology* 72: 896–903.
- Ives, A. R., B. Dennis, K. Cottingham, and S. Carpenter. 2003. "Estimating Community Stability and Ecological Interactions from Time-Series Data." *Ecological Monographs* 73: 301–30.
- Jackson, J. B., M. X. Kirby, W. H. Berger, K. A. Bjorndal, L. W. Botsford, B. J. Bourque, R. H. Bradbury, et al. 2001. "Historical Overfishing and the Recent Collapse of Coastal Ecosystems." *Science* 293: 629–37.
- Kéfi, S., V. Domnguez-Garcia, I. Donohue, C. Fontaine, E. Thébault, and V. Dakos. 2019. "Advancing our Understanding of Ecological Stability." *Ecology Letters* 22: 1349–56.
- Levin, S. A., and J. Lubchenco. 2008. "Resilience, Robustness, and Marine Ecosystem-Based Management." *Bioscience* 58: 27–32.
- Lu, M., K. Winner, and W. Jetz. 2021. "A Unifying Framework for Quantifying and Comparing n-Dimensional Hypervolumes." *Methods in Ecology and Evolution* 12: 1953–68.
- Medeiros, L. P., S. Allesina, V. Dakos, G. Sugihara, and S. Saavedra. 2023. "Ranking Species Based on Sensitivity to Perturbations

- under Non-equilibrium Community Dynamics." *Ecology Letters* 26: 170–83.
- Medeiros, L. P., and S. Saavedra. 2023. "Species-Correlated-Responses." Zenodo. <https://doi.org/10.5281/zenodo.7968611>.
- Medeiros, L. P., C. Song, and S. Saavedra. 2021. "Merging Dynamical and Structural Indicators to Measure Resilience in Multispecies Systems." *Journal of Animal Ecology* 90: 2027–40.
- Munch, S. B., A. Brias, G. Sugihara, and T. L. Rogers. 2020. "Frequently Asked Questions about Nonlinear Dynamics and Empirical Dynamic Modelling." *ICES Journal of Marine Science* 77: 1463–79.
- Neubert, M. G., and H. Caswell. 1997. "Alternatives to Resilience for Measuring the Responses of Ecological Systems to Perturbations." *Ecology* 78: 653–65.
- Pennekamp, F., A. C. Iles, J. Garland, G. Brennan, U. Brose, U. Gaedke, U. Jacob, et al. 2019. "The Intrinsic Predictability of Ecological Time Series and its Potential to Guide Forecasting." *Ecological Monographs* 89: e01359.
- Pennekamp, F., M. Pontarp, A. Tabi, F. Altermatt, R. Alther, Y. Choffat, E. A. Fronhofer, et al. 2018. "Biodiversity Increases and Decreases Ecosystem Stability." *Nature* 563: 109–12.
- Pimm, S. L. 1984. "The Complexity and Stability of Ecosystems." *Nature* 307: 321–6.
- Pires, M. M., J. L. O'Donnell, L. A. Burkle, C. Daz-Castelazo, D. H. Hembry, J. D. Yeakel, E. A. Newman, L. P. Medeiros, M. A. de Aguiar, and P. R. Guimarães, Jr. 2020. "The Indirect Paths to Cascading Effects of Extinctions in Mutualistic Networks." *Ecology* 101: e03080.
- Pringle, R. M., T. P. Young, D. I. Rubenstein, and D. J. McCauley. 2007. "Herbivore-Initiated Interaction Cascades and their Modulation by Productivity in an African Savanna." *Proceedings of the National Academy of Sciences* 104: 193–7.
- Rogers, T. L., S. B. Munch, S.-I. S. Matsuzaki, and C. C. Symons. 2023. "Intermittent Instability Is Widespread in Plankton Communities." *Ecology Letters* 26: 470–81.
- Saavedra, S., R. P. Rohr, J. Bascompte, O. Godoy, N. J. B. Kraft, and J. M. Levine. 2017. "A Structural Approach for Understanding Multispecies Coexistence." *Ecological Monographs* 87: 470–86.
- Samhouri, J. F., A. C. Stier, S. M. Hennessey, M. Novak, B. S. Halpern, and P. S. Levin. 2017. "Rapid and Direct Recoveries of Predators and Prey through Synchronized Ecosystem Management." *Nature Ecology & Evolution* 1: 1–6.
- Schneider, F. D., S. Scheu, and U. Brose. 2012. "Body Mass Constraints on Feeding Rates Determine the Consequences of Predator Loss." *Ecology Letters* 15: 436–43.
- Song, C., and S. Saavedra. 2021. "Bridging Parametric and Nonparametric Measures of Species Interactions Unveils New Insights of Non-equilibrium Dynamics." *Oikos* 130: 1027–34.
- Strang, G. 2016. *Introduction to Linear Algebra*. Wellesley: Wellesley-Cambridge Press.
- Strogatz, S. H. 2018. *Nonlinear Dynamics and Chaos: With Applications to Physics, Biology, Chemistry, and Engineering*. Boca Raton: CRC press.
- Sugihara, G. 1994. "Nonlinear Forecasting for the Classification of Natural Time Series. Philosophical Transactions of the Royal Society of London." *Series A: Physical and Engineering Sciences* 348: 477–95.
- Tilman, D., P. B. Reich, and J. M. Knops. 2006. "Biodiversity and Ecosystem Stability in a Decade-Long Grassland Experiment." *Nature* 441: 629–32.
- Turner, M. G., V. H. Dale, and E. H. Everham. 1997. "Fires, Hurricanes, and Volcanoes: Comparing Large Disturbances." *Bioscience* 47: 758–68.
- Upadhyay, R. 2000. "Chaotic Behaviour of Population Dynamic Systems in Ecology." *Mathematical and Computer Modelling* 32: 1005–15.
- Ushio, M., C.-H. Hsieh, R. Masuda, E. R. Deyle, H. Ye, C.-W. Chang, G. Sugihara, and M. Kondoh. 2018. "Fluctuating Interaction Network and Time-Varying Stability of a Natural Fish Community." *Nature* 554: 360–3.
- Vano, J., J. Wildenberg, M. Anderson, J. Noel, and J. Sprott. 2006. "Chaos in Low-Dimensional Lotka-Volterra Models of Competition." *Nonlinearity* 19: 2391–404.
- White, L., N. E. O'Connor, Q. Yang, M. C. Emmerson, and I. Donohue. 2020. "Individual Species Provide Multifaceted Contributions to the Stability of Ecosystems." *Nature Ecology & Evolution* 4: 1–8.
- Wootton, J. T. 1994. "The Nature and Consequences of Indirect Effects in Ecological Communities." *Annual Review of Ecology and Systematics* 25: 443–66.
- Worsfold, N. T., P. H. Warren, and O. L. Petchey. 2009. "Context-Dependent Effects of Predator Removal from Experimental Microcosm Communities." *Oikos* 118: 1319–26.
- Ye, H., R. J. Beamish, S. M. Glaser, S. C. Grant, C.-H. Hsieh, L. J. Richards, J. T. Schnute, and G. Sugihara. 2015. "Equation-Free Mechanistic Ecosystem Forecasting Using Empirical Dynamic Modeling." *Proceedings of the National Academy of Sciences* 112: E1569–76.
- Yodzis, P. 1989. *Introduction to Theoretical Ecology*. New York: HarperCollins College Division.

SUPPORTING INFORMATION

Additional supporting information can be found online in the Supporting Information section at the end of this article.

How to cite this article: Medeiros, Lucas P., and Serguei Saavedra. 2023. "Understanding the State-Dependent Impact of Species Correlated Responses on Community Sensitivity to Perturbations." *Ecology* e4115. <https://doi.org/10.1002/ecy.4115>

Appendix S1

Understanding the state-dependent impact of species correlated responses on community sensitivity to perturbations

Lucas P. Medeiros and Serguei Saavedra

Journal: *Ecology*

Section S1: Derivation of expectation and covariance matrix of perturbed abundances

Here, we derive the linear dynamics of small perturbations as well as the expectation and covariance matrix describing the distribution of these perturbations in the absence of a stable fixed point. Following the main text, we write the generic population dynamics of a community with S species as: $\frac{d\mathbf{N}}{dt} = \mathbf{f}(\mathbf{N})$, where $\mathbf{N} = [N_1, \dots, N_S]^\top$ is the vector of species abundances and $\mathbf{f} = (f_1, \dots, f_S)$ ($f_i: \mathbb{R}^S \rightarrow \mathbb{R}$) is a set of functions describing species abundance growth rates. Note that each f_i also depends on a set of parameters, which we consider to be fixed over time. At any given state \mathbf{N} , a pulse perturbation $\mathbf{p} = [p_1, \dots, p_S]^\top$ may change species abundances

from \mathbf{N} into $\tilde{\mathbf{N}}$ (i.e., $\tilde{\mathbf{N}} = \mathbf{N} + \mathbf{p}$) (Bender et al., 1984). We can obtain the linearized dynamics of a small perturbation \mathbf{p} by computing the Taylor expansion of $\frac{d\tilde{\mathbf{N}}}{dt}$ around \mathbf{N} (Medeiros et al., 2023, Strogatz, 2018):

$$\frac{d\tilde{\mathbf{N}}}{dt} = \mathbf{f}(\mathbf{N}) + \frac{\partial \mathbf{f}}{\partial \tilde{\mathbf{N}}} \Big|_{\tilde{\mathbf{N}}=\mathbf{N}} \cdot (\tilde{\mathbf{N}} - \mathbf{N}) + O(\mathbf{p}^\top \mathbf{p}), \quad [\text{S1}]$$

where $\frac{\partial \mathbf{f}}{\partial \mathbf{N}} = \mathbf{J}$ is the Jacobian matrix of partial derivatives with $j_{ij} = \frac{\partial f_i}{\partial N_j}$ (interspecific effects), which is evaluated at \mathbf{N} . If \mathbf{p} is small, we can approximate its dynamics by taking just the linear term (i.e., ignoring higher-order terms):

$$\begin{aligned} \frac{d\tilde{\mathbf{N}}}{dt} &= \mathbf{f}(\mathbf{N}) + \frac{\partial \mathbf{f}}{\partial \tilde{\mathbf{N}}} \Big|_{\tilde{\mathbf{N}}=\mathbf{N}} \cdot (\tilde{\mathbf{N}} - \mathbf{N}) \\ \frac{d\mathbf{N}}{dt} + \frac{d\mathbf{p}}{dt} &= \frac{d\mathbf{N}}{dt} + \mathbf{J}|_{\tilde{\mathbf{N}}=\mathbf{N}} \cdot \mathbf{p} \\ \frac{d\mathbf{p}}{dt} &= \mathbf{J}|_{\tilde{\mathbf{N}}=\mathbf{N}} \cdot \mathbf{p}. \end{aligned} \quad [\text{S2}]$$

Therefore, the dynamics of a small perturbation \mathbf{p} can be approximated by the linear equation above (Medeiros et al., 2023, Strogatz, 2018). Note that we have not assumed the existence of a stable fixed point here (i.e., $\mathbf{N} = \mathbf{N}^*$ with $\mathbf{f}(\mathbf{N}^*) = \mathbf{0}$) and, therefore, equation [S2] is valid even when abundances are changing over time (e.g., under transients, cycles, or chaos). Importantly, also note that \mathbf{J} can change over time because it depends on species abundances (\mathbf{N} ; i.e., state-dependent). For a given \mathbf{N} vector at a given time t , we can obtain the solution for equation [S2] over a short time period k by assuming that \mathbf{J} does not change much from t to $t+k$: $\mathbf{p}(t+k) = e^{k\mathbf{J}}\mathbf{p}(t)$, where $e^{\mathbf{A}} = \sum_{i=1}^{\infty} \frac{1}{i!} \mathbf{A}^i$ is the exponential of matrix \mathbf{A} (Arnoldi et al., 2018, Medeiros et al., 2023).

As described in the main text, we often have no knowledge of how perturbations will affect a given community at a given time. Thus, we assume that pulse perturbations at an arbitrary

time t ($\mathbf{p}(t)$) follow a distribution with mean vector $\boldsymbol{\mu}_t$ and covariance matrix Σ_t (Figure 2a).

Although this is not necessary for the derivations below, we focus on perturbations that are not biased in a given direction (i.e., $\boldsymbol{\mu}_t = \mathbf{0}$) and perturbations that affect each species equally and independently (i.e., $\Sigma_t = c\mathbf{I}$, where c is a constant and \mathbf{I} is the identity matrix). By defining $\mathbf{M} = e^{k\mathbf{J}}$, we can derive the mean vector of the distribution of perturbations at time $t + k$ (Medeiros et al., 2023):

$$\begin{aligned}\mathbb{E}[\mathbf{p}(t+k)] &= \mathbb{E}[\mathbf{M}\mathbf{p}(t)] \\ &= \mathbf{M}\mathbb{E}[\mathbf{p}(t)] \\ &= \mathbf{M}\boldsymbol{\mu}_t,\end{aligned}\quad [\text{S3}]$$

where $\mathbb{E}[\mathbf{X}] = [\mathbb{E}[X_1], \dots, \mathbb{E}[X_n]]^\top$ is the vector of expected values for the random vector $\mathbf{X} = [X_1, \dots, X_n]^\top$. Note that if $\boldsymbol{\mu}_t = \mathbf{0}$, then $\mathbb{E}[\mathbf{p}(t+k)] = \mathbf{0}$ (i.e., perturbations remain unbiased). In the special case where $\mathbf{p}(t)$ follows a multivariate normal distribution, $\mathbf{p}(t+k)$ also follows a multivariate normal distribution because $\mathbf{M}\mathbf{p}(t)$ is a weighted sum of normal distributions. Most importantly, we can also derive the covariance matrix of $\mathbf{p}(t+k)$, which we denote as Σ (Arnoldi et al., 2018, Medeiros et al., 2023):

$$\begin{aligned}\Sigma &= \mathbb{E}[(\mathbf{p}(t+k) - \mathbb{E}[\mathbf{p}(t+k)])(\mathbf{p}(t+k) - \mathbb{E}[\mathbf{p}(t+k)])^\top] \\ &= \mathbf{M}\mathbb{E}[(\mathbf{p}(t) - \mathbb{E}[\mathbf{p}(t)])(\mathbf{p}(t) - \mathbb{E}[\mathbf{p}(t)])^\top]\mathbf{M}^\top \\ &= \mathbf{M}\Sigma_t\mathbf{M}^\top,\end{aligned}\quad [\text{S4}]$$

where $\mathbb{E}[(\mathbf{X} - \mathbb{E}[\mathbf{X}])(\mathbf{X} - \mathbb{E}[\mathbf{X}])^\top]$ is the definition of the covariance matrix for the random vector \mathbf{X} . The ij th element of this matrix contains the covariance between random variable X_i and X_j : $\text{cov}(X_i, X_j) = \mathbb{E}[(X_i - \mathbb{E}[X_i])(X_j - \mathbb{E}[X_j])]$. Thus, Σ is obtained via a transformation of the

initial covariance matrix (Σ_t) due to interspecific effects present in the Jacobian matrix \mathbf{J} (Figure 2a). Note that, in addition to knowing \mathbf{J} , knowledge of Σ_t and k is required to compute Σ . The accuracy of Σ in describing the distribution of perturbed abundances has been verified under a stable fixed point (Arnoldi et al., 2018) and in the next section we describe our simulations that confirm this accuracy under cyclic or chaotic dynamics (Figure S1).

Section S2: Accuracy of covariance matrix in describing perturbed abundances

We perform perturbation simulations to verify the accuracy of the covariance matrix $\Sigma = e^{k\mathbf{J}}\Sigma_t e^{k\mathbf{J}^\top}$ (see previous section) in describing the distribution of perturbed abundances ($\tilde{\mathbf{N}} = \mathbf{N} + \mathbf{p}$). To do so, we use the three synthetic multivariate time series with 250 points ($\{\mathbf{N}(t)\}$, $t = 1, \dots, 250$) generated from the population dynamics models described in the main text (see *Materials and Methods* section). For each time series, we apply 300 pulse perturbations ($\mathbf{p} \sim \mathcal{N}(\boldsymbol{\mu}_t, \Sigma_t)$) at each state $\mathbf{N}(t)$. We assume that perturbations are independent for each species (i.e., covariances in Σ_t are zero) and are centered in $\mathbf{N}(t)$ (i.e., $\boldsymbol{\mu}_t$ is zero). We also assume that the standard deviation of perturbations (i.e., square root of diagonal elements of Σ_t) is the same for every species and is set as 15% of the mean standard deviation of species abundances: $0.15\frac{1}{S} \sum_{i=1}^S \sigma_{N_i}$, where σ_{N_i} is the standard deviation of N_i for the whole time series. After applying perturbations, we evolve each perturbed state $\tilde{\mathbf{N}}$ over time for k time steps. We set $k = 3$ for the 2-species predator-prey model (equation [2] in the main text), $k = 0.5$ for the 3-species food chain model (equation [3] in the main text), and $k = 3$ for the 4-species competition model (equation [4] in the main text). An example of these perturbed abundances ($\tilde{\mathbf{N}}$) at the initial time t and final time $t + k$ can be seen in Figure 2b in the main text (initial: light purple

points; final: dark purple points).

For each time series and each state $\mathbf{N}(t)$, we compute Σ using the analytical Jacobian matrix \mathbf{J} evaluated at $\mathbf{N}(t)$ as well as k and Σ_t used in the perturbation simulations. Then, we compute the data covariance matrix \mathbf{S} using the 300 perturbed abundances at time $t+k$ ($\tilde{\mathbf{N}}(t+k)$). That is, the ij th element of \mathbf{S} contains the covariance between species i ($\tilde{N}_i(t+k)$) and species j ($\tilde{N}_j(t+k)$) computed from the set of perturbed abundances (e.g., dark purple points in Figure 2b in the main text). Figure S1 shows, for each population dynamics model, the elements of \mathbf{S} (red lines) and of Σ (blue lines) over time. We find a strong correlation over time between the elements of these two matrices for all models: 2-species predator-prey model: 0.87 ± 0.10 (mean \pm standard deviation), 3-species food chain model: 0.91 ± 0.04 , and 4-species competition model: 0.88 ± 0.03 . These strong correlations confirm that Σ captures how the distribution of perturbed abundances changes over time for each state along an attractor.

Section S3: Determinant of covariance matrix

In the main text, we state that the determinant of a covariance matrix can always be written as the product of variances times the determinant of the correlation matrix. Here, we provide a mathematical proof for this statement and also prove that the determinant of the correlation matrix is always between 0 and 1. Let us define a generic $S \times S$ covariance matrix as the following symmetric and positive semi-definite matrix:

$$\Sigma = \begin{bmatrix} \sigma_1^2 & \sigma_{12}^2 & \cdots & \sigma_{1S}^2 \\ \sigma_{12}^2 & \sigma_2^2 & \cdots & \sigma_{2S}^2 \\ \vdots & \vdots & \ddots & \vdots \\ \sigma_{1S}^2 & \sigma_{2S}^2 & \cdots & \sigma_{SS}^2 \end{bmatrix},$$

where σ_i^2 is the variance of variable i and σ_{ij}^2 is the covariance between variables i and j . Note that the correlation between i and j is given by: $\rho_{ij} = \frac{\sigma_{ij}^2}{\sigma_i \sigma_j}$. This allows us to rewrite Σ as:

$$\Sigma = \begin{bmatrix} \sigma_1^2 & \rho_{12}\sigma_1\sigma_2 & \cdots & \rho_{1S}\sigma_1\sigma_S \\ \rho_{12}\sigma_1\sigma_2 & \sigma_2^2 & \cdots & \rho_{2S}\sigma_2\sigma_S \\ \vdots & \vdots & \ddots & \vdots \\ \rho_{1S}\sigma_1\sigma_S & \rho_{2S}\sigma_2\sigma_S & \cdots & \sigma_S^2 \end{bmatrix}.$$

Let us denote the determinant of an arbitrary matrix \mathbf{A} as $|\mathbf{A}|$. Now, we can use the fact that if a constant c multiplies the entire i th column (or row) of \mathbf{A} , then: $|\mathbf{A}| = c|\mathbf{A}'|$, where \mathbf{A}' is matrix \mathbf{A} after dividing all elements in column (or row) i by c . Because each σ_i multiplies the entire i th column of Σ , we have that:

$$|\Sigma| = \prod_{i=1}^S \sigma_i \cdot \begin{vmatrix} \sigma_1 & \rho_{12}\sigma_1 & \cdots & \rho_{1S}\sigma_1 \\ \rho_{12}\sigma_2 & \sigma_2 & \cdots & \rho_{2S}\sigma_2 \\ \vdots & \vdots & \ddots & \vdots \\ \rho_{1S}\sigma_S & \rho_{2S}\sigma_S & \cdots & \sigma_S \end{vmatrix}.$$

In addition, because each σ_i multiplies the entire i th row of Σ , we have that:

$$|\Sigma| = \prod_{i=1}^S \sigma_i^2 \cdot \begin{vmatrix} 1 & \rho_{12} & \cdots & \rho_{1S} \\ \rho_{12} & 1 & \cdots & \rho_{2S} \\ \vdots & \vdots & \ddots & \vdots \\ \rho_{1S} & \rho_{2S} & \cdots & 1 \end{vmatrix} = \prod_{i=1}^S \sigma_i^2 \cdot |\mathbf{P}|,$$

where \mathbf{P} is the correlation matrix. Thus, this proves that $|\Sigma| = \prod_{i=1}^S \sigma_i^2 \cdot |\mathbf{P}|$. In particular, if we take the logarithm of this expression, we obtain equation [1] in the main text, which consists of

our decomposition of the community sensitivity to perturbations into contributions of individual species and of species correlations.

In addition, we can prove that $0 \leq |\mathbf{P}| \leq 1$ and, therefore, species correlations can only decrease community sensitivity. Without correlations (i.e., $\rho_{ij} = 0 \forall i \neq j$), we have that $\mathbf{P} = \mathbf{I}$, where \mathbf{I} is the identity matrix. Because in this case \mathbf{P} is a diagonal matrix, its determinant will be given by the product of its diagonal elements: $|\mathbf{P}| = 1$. This gives an upper bound for $|\mathbf{P}|$ as correlations will always decrease this determinant. To obtain the lower bound, we note that because \mathbf{P} is positive semi-definite, its determinant is always nonnegative. Therefore, we have proved that $0 \leq |\mathbf{P}| \leq 1$.

References

- Arnoldi, J.-F., A. Bideault, M. Loreau, and B. Haegeman. 2018. How ecosystems recover from pulse perturbations: A theory of short-to long-term responses. *Journal of theoretical biology*, **436**:79–92.
- Becks, L., F. M. Hilker, H. Malchow, K. Jürgens, and H. Arndt. 2005. Experimental demonstration of chaos in a microbial food web. *Nature*, **435**:1226–1229.
- Bender, E. A., T. J. Case, and M. E. Gilpin. 1984. Perturbation experiments in community ecology: theory and practice. *Ecology*, **65**:1–13.
- Blasius, B., L. Rudolf, G. Weithoff, U. Gaedke, and G. F. Fussmann. 2020. Long-term cyclic persistence in an experimental predator–prey system. *Nature*, **577**:226–230.
- Joe, H. 2006. Generating random correlation matrices based on partial correlations. *Journal of multivariate analysis*, **97**:2177–2189.
- Medeiros, L. P., S. Allesina, V. Dakos, G. Sugihara, and S. Saavedra. 2023. Ranking species based on sensitivity to perturbations under non-equilibrium community dynamics. *Ecology Letters*, **26**:170–183.
- Strogatz, S. H. 2018. Nonlinear dynamics and chaos: with applications to physics, biology, chemistry, and engineering. CRC press.

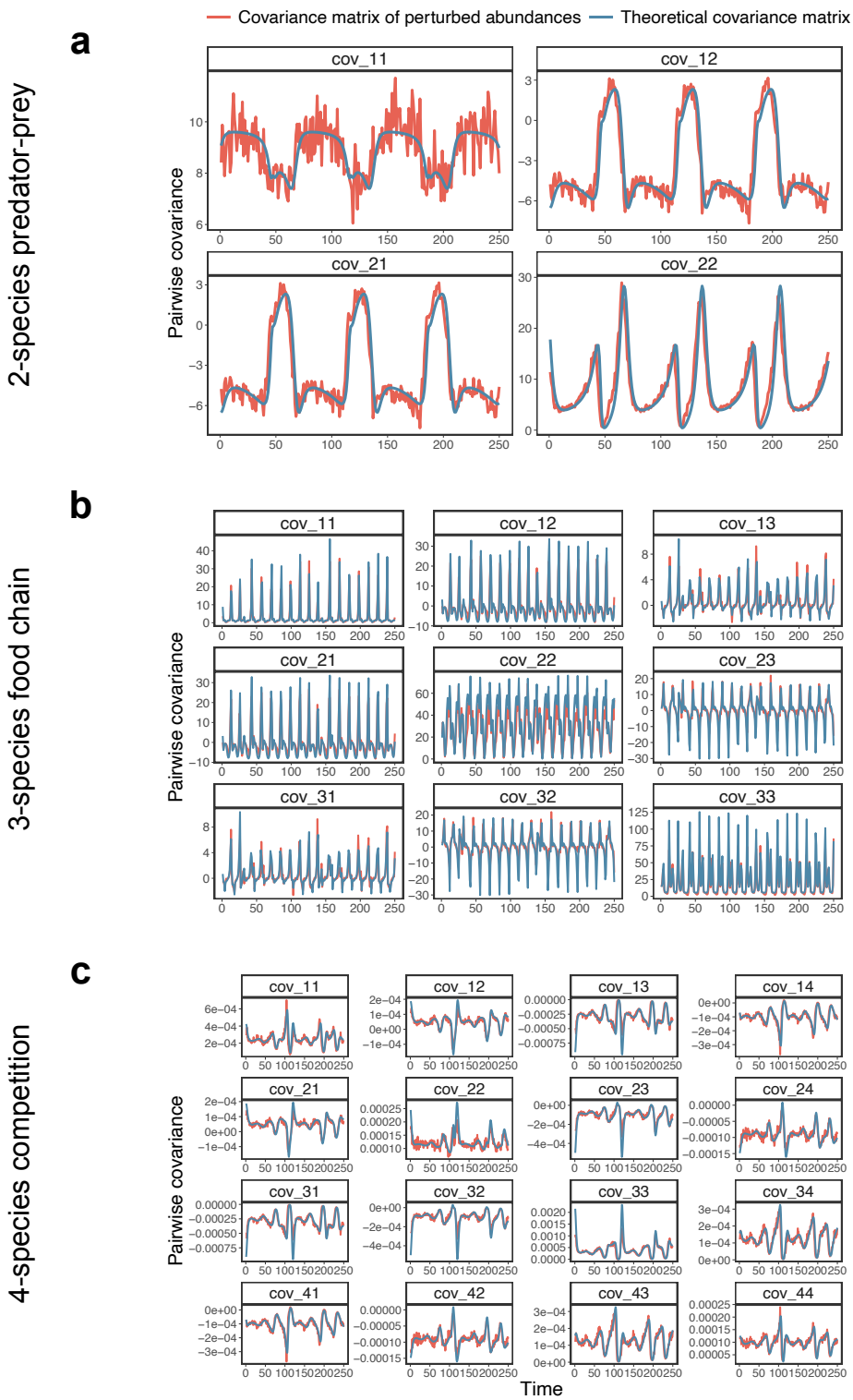


Figure S1. Accuracy of covariance matrix Σ in describing the distribution of perturbed abundances under cyclic or chaotic dynamics. **a-c**, Each panel shows the same element of \mathbf{S} (data covariance matrix, red line) and of Σ (blue line) over time. The mean (\pm standard deviation) correlation between an element of \mathbf{S} and an element of Σ (correlation between red and blue lines) is: 0.87 ± 0.10 for the 2-species predator-prey model (**a**, equation [2] in the main text), 0.91 ± 0.04 for the 3-species food chain model (**b**, equation [3] in the main text), and 0.88 ± 0.03 for the 4-species competition model (**c**, equation [4] in the main text).

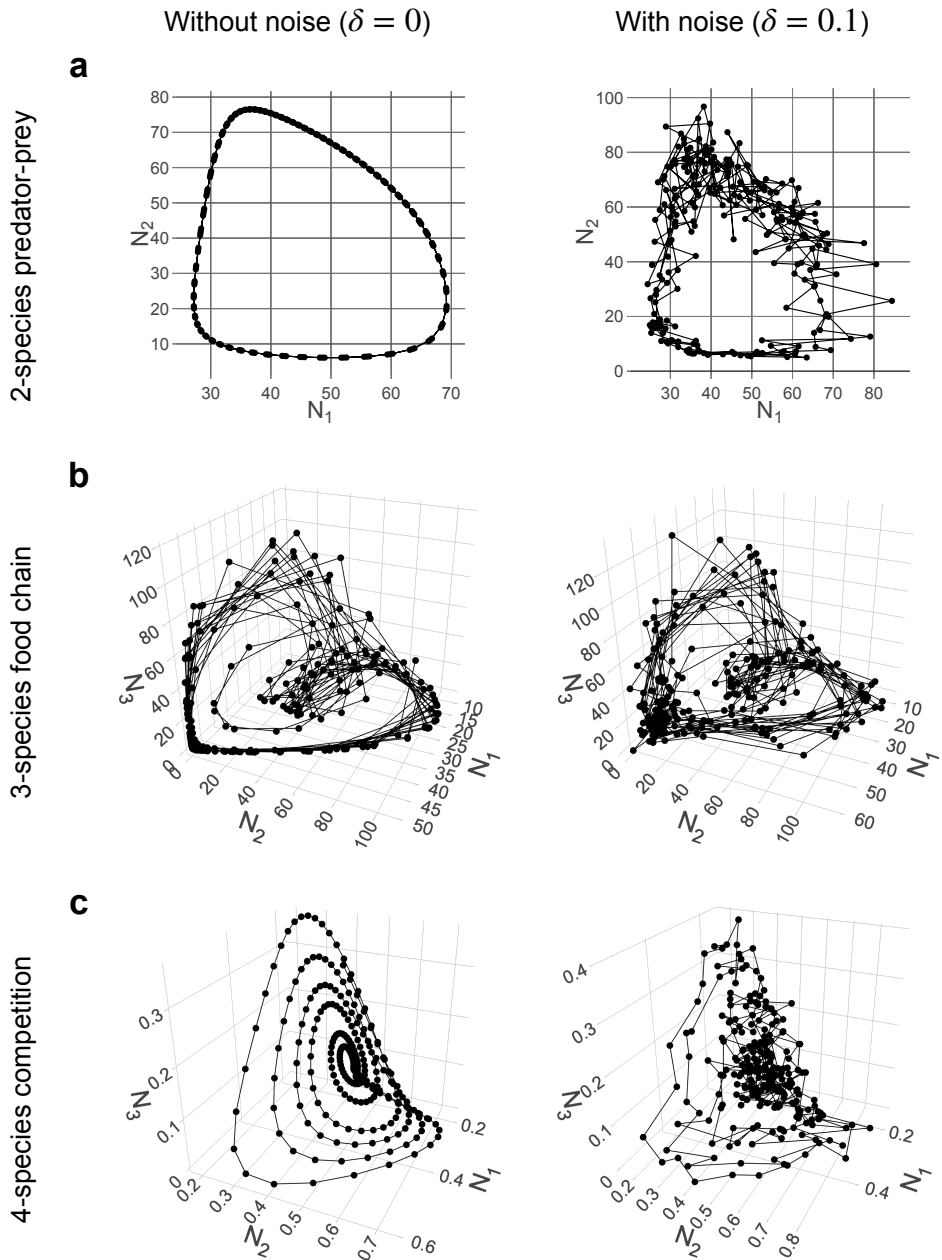


Figure S2. Cyclic and chaotic attractors in state space corresponding to each synthetic time series generated by a population dynamics model. **a-c**, Each plot shows the 250 points ($\{\mathbf{N}(t)\}$, $t = 1, \dots, 250$) generated by numerically integrating the indicated model and then sampling equidistant points. For the left column we did not add noise to the abundances, whereas for the right column we add 10% of Gaussian noise as described in the *Materials and Methods* section in the main text. In our analyses, we compute the analytical Jacobian matrix \mathbf{J} from the attractors without noise (left) and infer \mathbf{J} with the S-map from the attractors with noise (right). Note that we only show the abundances of species 1, 2, and 3 for the 4-species model.

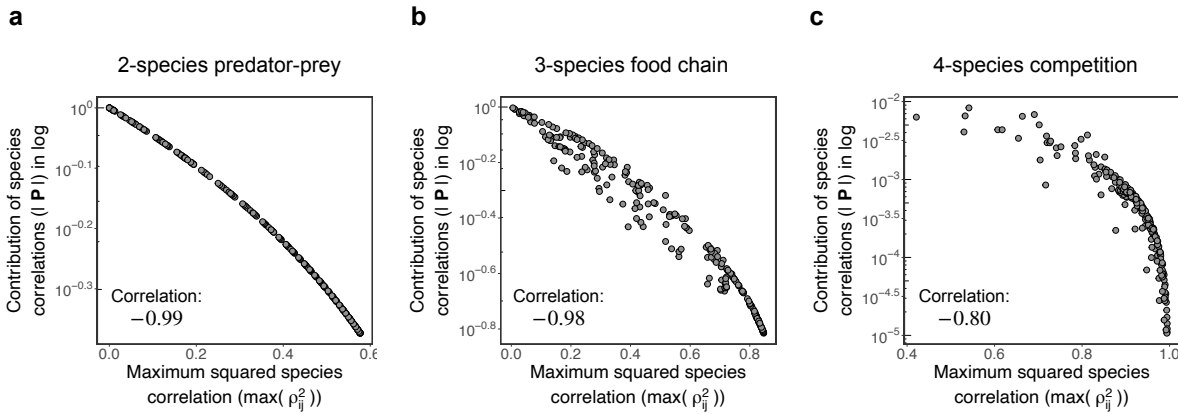


Figure S3. Contribution of species correlations ($\log |\mathbf{P}|$) is driven by the maximum squared correlation ($\max(\rho_{ij}^2)$). **a-c.** Each plot shows $\log |\mathbf{P}|$ and $\max(\rho_{ij}^2)$ computed at each state ($\mathbf{N}(t)$); each point corresponds to a state of the synthetic time series generated by the indicated population dynamics model. Note that the correlation matrix \mathbf{P} is computed from the covariance matrix Σ , which is in turn computed from the analytical Jacobian matrix \mathbf{J} (see *Materials and Methods* in the main text). The correlation between $\log |\mathbf{P}|$ and $\max(\rho_{ij}^2)$ is: -0.99 for the 2-species predator-prey model (**a**, equation [2] in the main text), -0.98 for the 3-species food chain model (**b**, equation [3] in the main text), and -0.80 for the 4-species competition model (**c**, equation [4] in the main text).

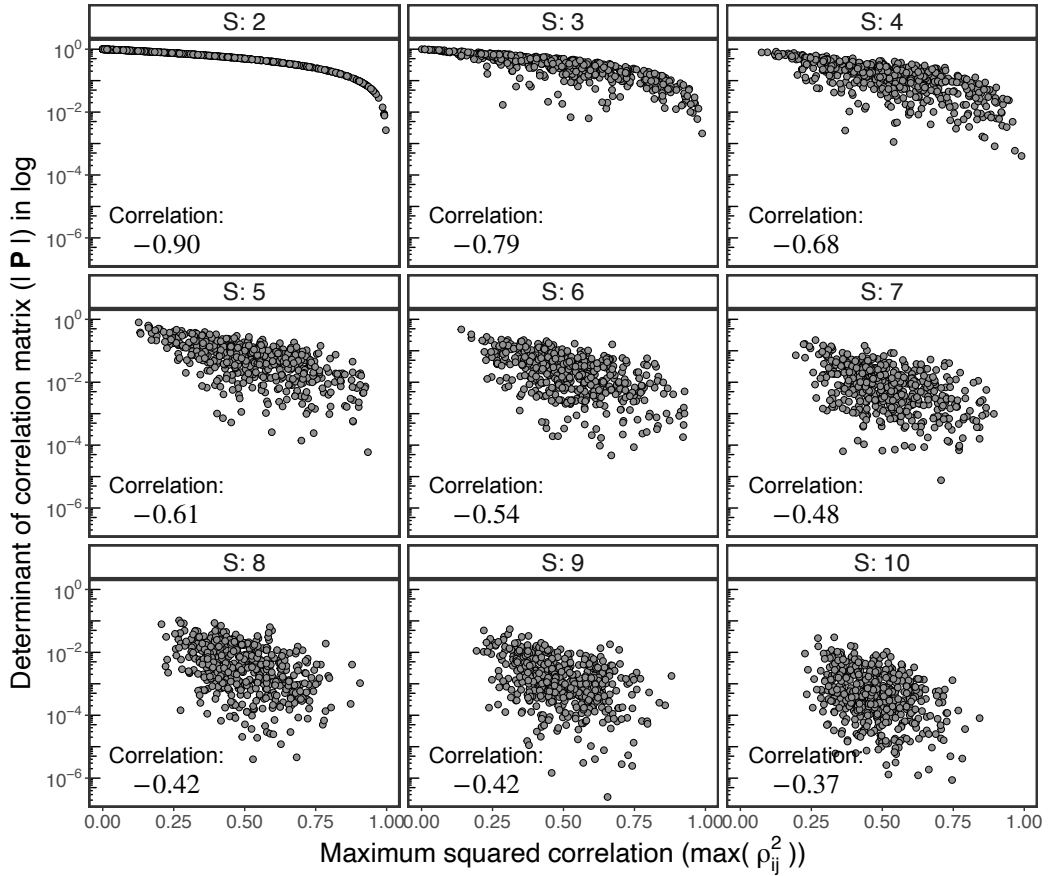


Figure S4. Log of determinant of correlation matrix ($\log |P|$) decreases with the maximum squared correlation ($\max(\rho_{ij}^2)$) for random correlation matrices. Each panel shows $\log |P|$ as a function of $\max(\rho_{ij}^2)$ for 500 randomly generated correlation matrices (each point denotes one matrix) with a given dimension S . Each matrix P was sampled uniformly over the space of positive definite correlation matrices (Joe, 2006). Note that, although the correlation between $\log |P|$ and $\max(\rho_{ij}^2)$ is strong for all values of S , it becomes weaker as S increases.

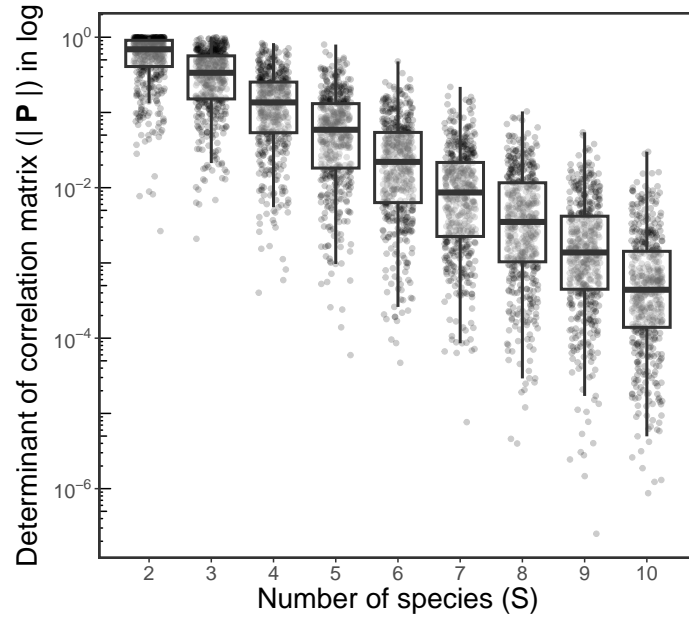


Figure S5. Log of determinant of correlation matrix ($\log |\mathbf{P}|$) decreases with the number of species (S) for random correlation matrices. We randomly generated 500 correlation matrices with a given dimension S and computed $\log |\mathbf{P}|$ for each matrix. Each point denotes one matrix and boxplots show the distribution of $\log |\mathbf{P}|$ for each S value. Each matrix \mathbf{P} was sampled uniformly over the space of positive definite correlation matrices (Joe, 2006).

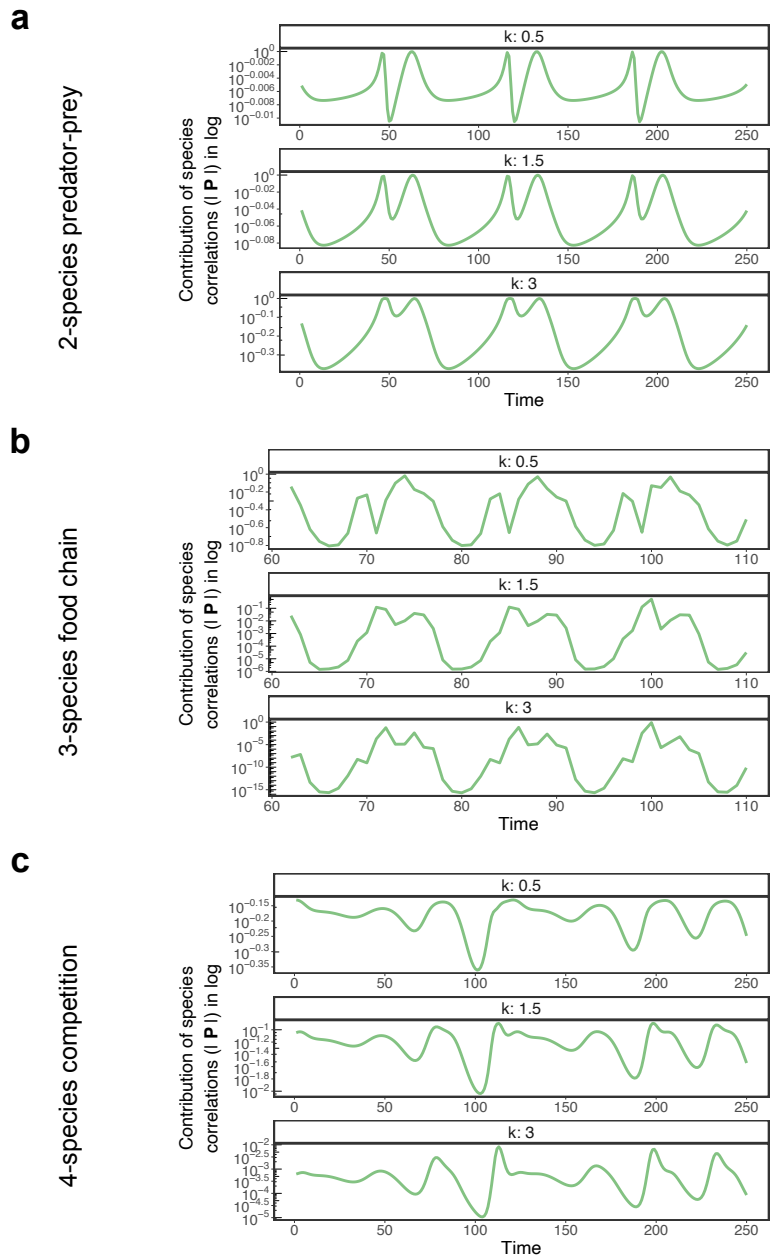
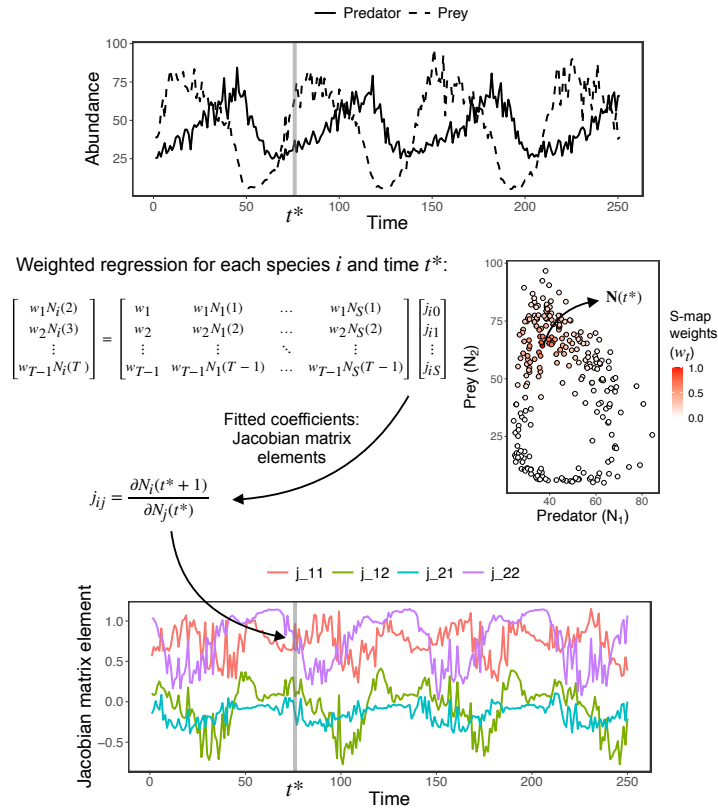


Figure S6. Contribution of species correlations ($\log |P|$) shows the same qualitative pattern over time for different values of k . **a-c,** Each plot shows $\log |P|$ over time computed using the analytical Jacobian matrix \mathbf{J} and a given value of the time step k (see *Materials and Methods* section in the main text). Note that the plots with $k = 3$ for the 2-species predator-prey (**a**) and the 4-species competition (**c**) models as well as the plot with $k = 0.5$ for the 3-species food chain model are identical to the center panels in Figure 3 in the main text.

a Infer Jacobian matrix from time series with S-map



b Perform community sensitivity decomposition

Community sensitivity decomposition for each time t^* :

- (1) Compute covariance matrix of perturbed abundances: $\Sigma = e^{k\mathbf{J}} \boldsymbol{\Sigma}_t e^{k\mathbf{J}^\top}$
- (2) Compute community sensitivity: $\log |\Sigma|$
- (3) Compute contribution of individual species: $\sum_{i=1}^S \log \sigma_i^2$
- (4) Compute contribution of species correlations: $\log |\mathbf{P}| = \log |\Sigma| - \sum_{i=1}^S \log \sigma_i^2$

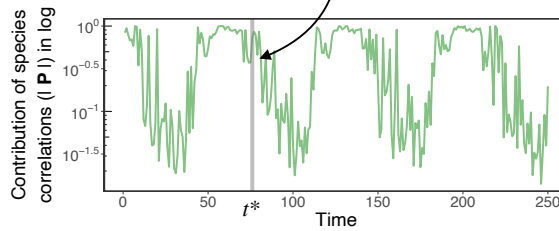


Figure S7. Illustration of our procedure to infer the time-varying Jacobian matrix and perform the community sensitivity decomposition. **a** (top), Time series (with 10% of observational noise) of the 2-species predator-prey model (equation [2] in the main text). We highlight time t^* as an example. **a** (center), Weighted regression equation of the S-map, which is fitted separately for each species i and time t^* . In this example, we have $S = 2$ and $T = 250$. For each time t^* , we obtain the Jacobian matrix elements: $j_{ij} = \frac{\partial N_i(t^* + 1)}{\partial N_j(t^*)}$. On the right, we show how we weight each point when performing the S-map for time t^* . **a** (bottom), Time series of inferred Jacobian matrix elements for the predator-prey system. **b** (top), Steps to perform our community sensitivity decomposition. For the first step, we use the inferred Jacobian matrix (\mathbf{J}) and specify an initial covariance matrix ($\boldsymbol{\Sigma}_t$) and a time step (k). In this example, we use $\boldsymbol{\Sigma}_t$ as the identity matrix and $k = 3$. **b** (bottom), Time series of the contribution of species correlations ($\log |\mathbf{P}|$) for the predator-prey system. Note that this plot is exactly the same as the bottom panel in Figure 4a in the main text.

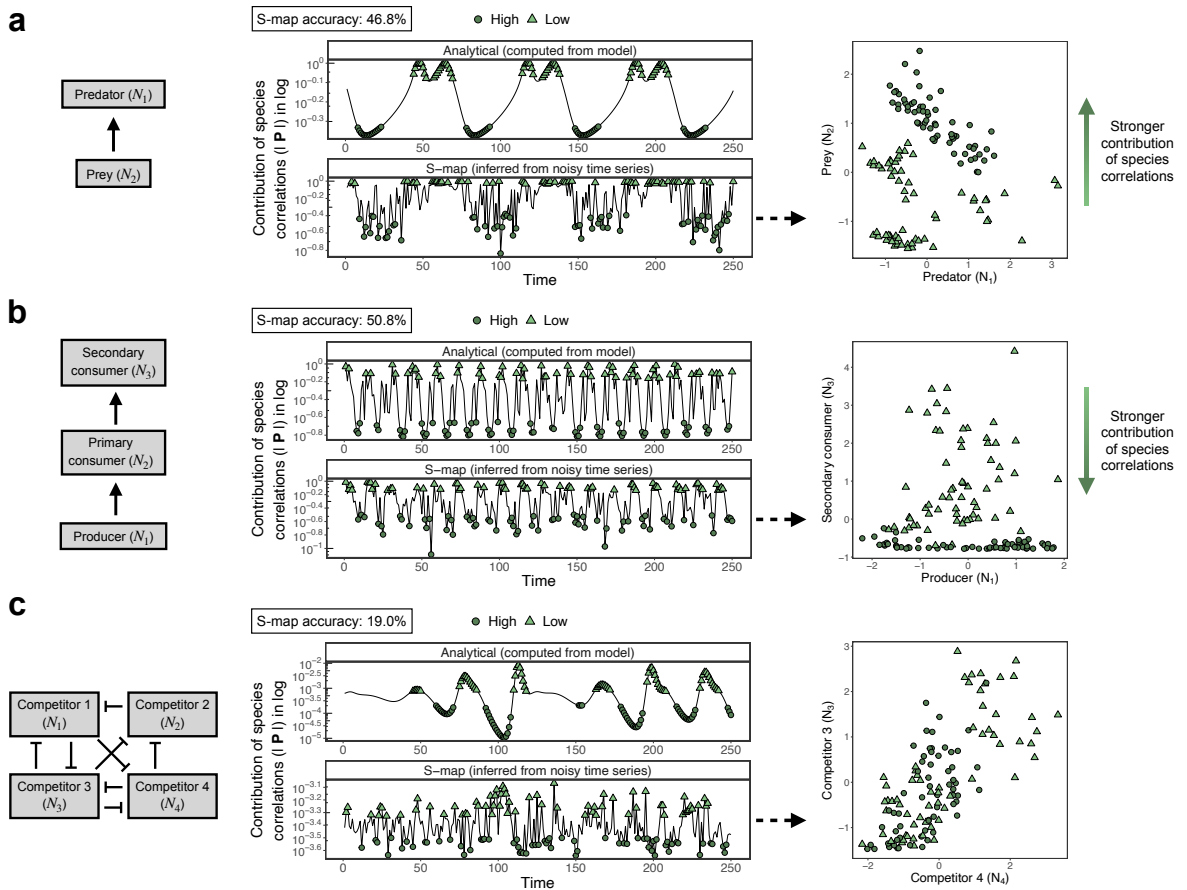


Figure S8. State-dependent impact of species correlated responses can be inferred directly from time series with a high amount of noise in species abundances. This figure is similar to Figure 4 in the main text, but here we performed the S-map to infer the Jacobian matrix \mathbf{J} using time series with 20% instead of 10% of observational noise (see *Materials and Methods* section in the main text). Note that the top center panels in **a**, **b**, and **c** (i.e., $\log |\mathbf{P}|$ computed analytically from model) are identical to the corresponding panels in Figure 4.

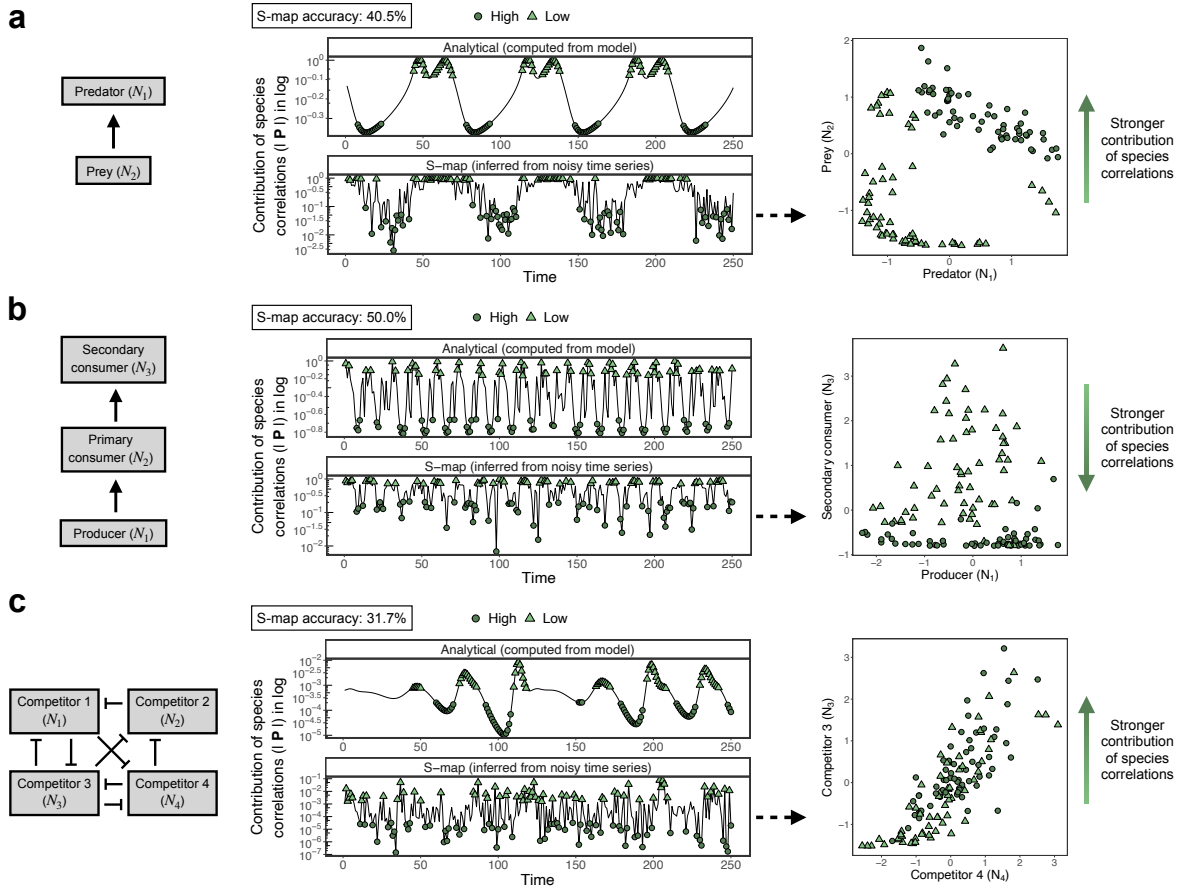


Figure S9. State-dependent impact of species correlated responses can be inferred directly from time series with noise in Σ_t and k . This figure is similar to Figure 4 in the main text, but here we added noise to the covariance matrix of perturbations at time t (Σ_t) and to the time step k before using Σ_t and k to compute the covariance matrix of perturbations at time $t + k$ (Σ , see *Materials and Methods* section in the main text) with the S-map. Specifically, for each time series point ($N(t)$), we added 20% of Gaussian noise to the diagonal elements of Σ_t (i.e., perturbation variances) and to k and then used the noisy Σ_t and k to compute Σ , which was in turn used to compute $\log |P|$. Note that we only added noise when computing Σ with the S-map and the top center panels in **a**, **b**, and **c** (i.e., $\log |P|$ computed analytically from model) are identical to the corresponding panels in Figure 4. Also note that there is also 10% of observational noise in species abundances in addition to noise in Σ_t and k .

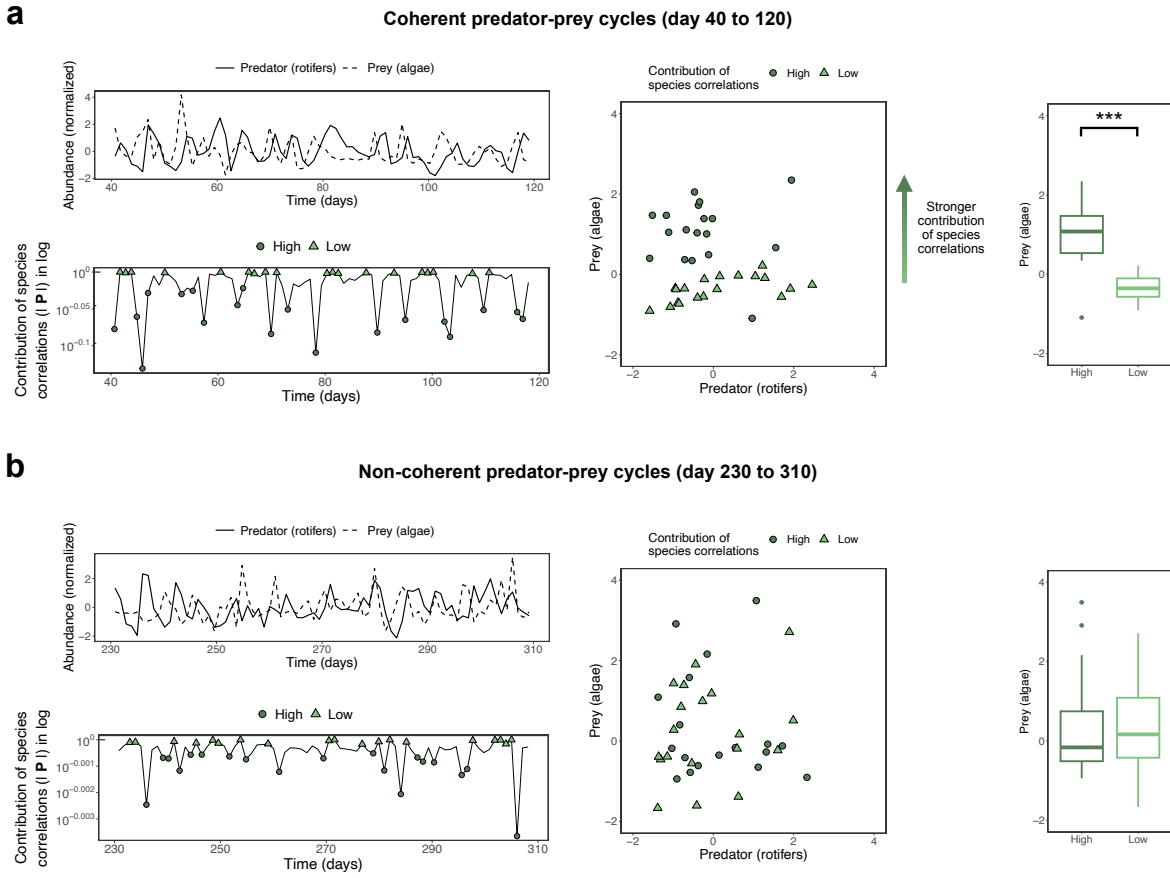


Figure S10. Impact of species correlated responses depends on prey abundance only under coherent predator-prey cycles. This figure is similar to Figure 5a in the main text (i.e., 2-species predator-prey data from Blasius et al. (2020)), but here we use one window of time (day 40 to 120) showing coherent predator-prey cycles (**a**) and one window of time (day 230 to 310) showing non-coherent cycles (**b**). Under coherent cycles (**a**), prey abundance is higher when the contribution of species correlations is high than when it is low (two sample t-test: $t(20.98) = 6.33, p < 0.0001$), similarly to Figure 5a. Under non-coherent cycles (**b**), we find no relationship between prey abundance and the contribution of species correlations (two sample t-test: $t(35.70) = 0.25, p = 0.8$).

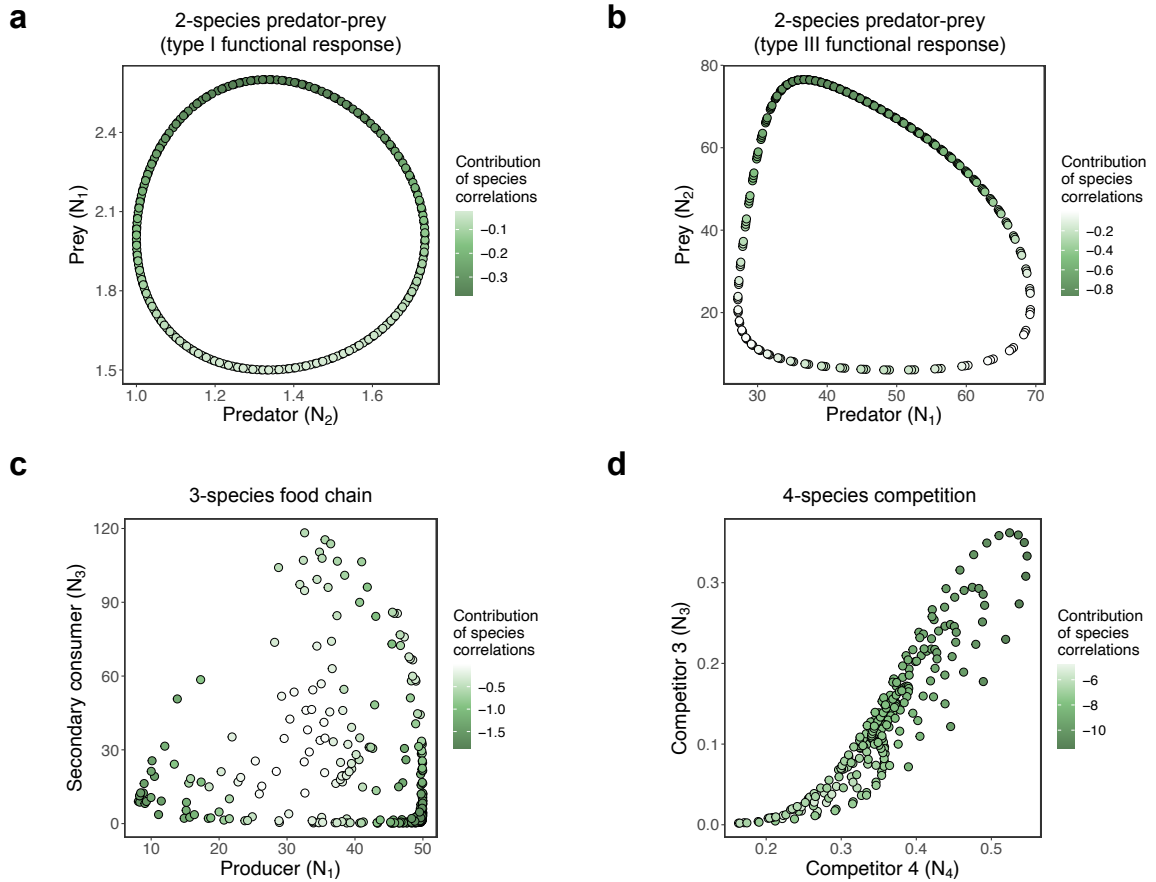


Figure S11. Contribution of species correlations ($\log |\mathbf{P}|$) across state space under four different population dynamics models. **a-d**, Each plot shows the attractor in state space corresponding to a given synthetic time series generated by the indicated population dynamics model. Each abundance state $\mathbf{N}(t)$ (i.e., each point) is colored according to $\log |\mathbf{P}|$ computed analytically from the model (see *Materials and Methods* in the main text). Note that panel **a** depicts a Lotka-Volterra predator-prey model (not shown in the main text) generated using the following parameters in equation [4] in the main text: $S = 2$, $r_1 = 0.2$, $r_2 = -0.2$, $a_{11} = 0$, $a_{12} = -0.15$, $a_{21} = 0.1$, and $a_{22} = 0$. Importantly, note that for both 2-species predator-prey models (**a** and **b**), $\log |\mathbf{P}|$ is higher when the prey abundance is higher.

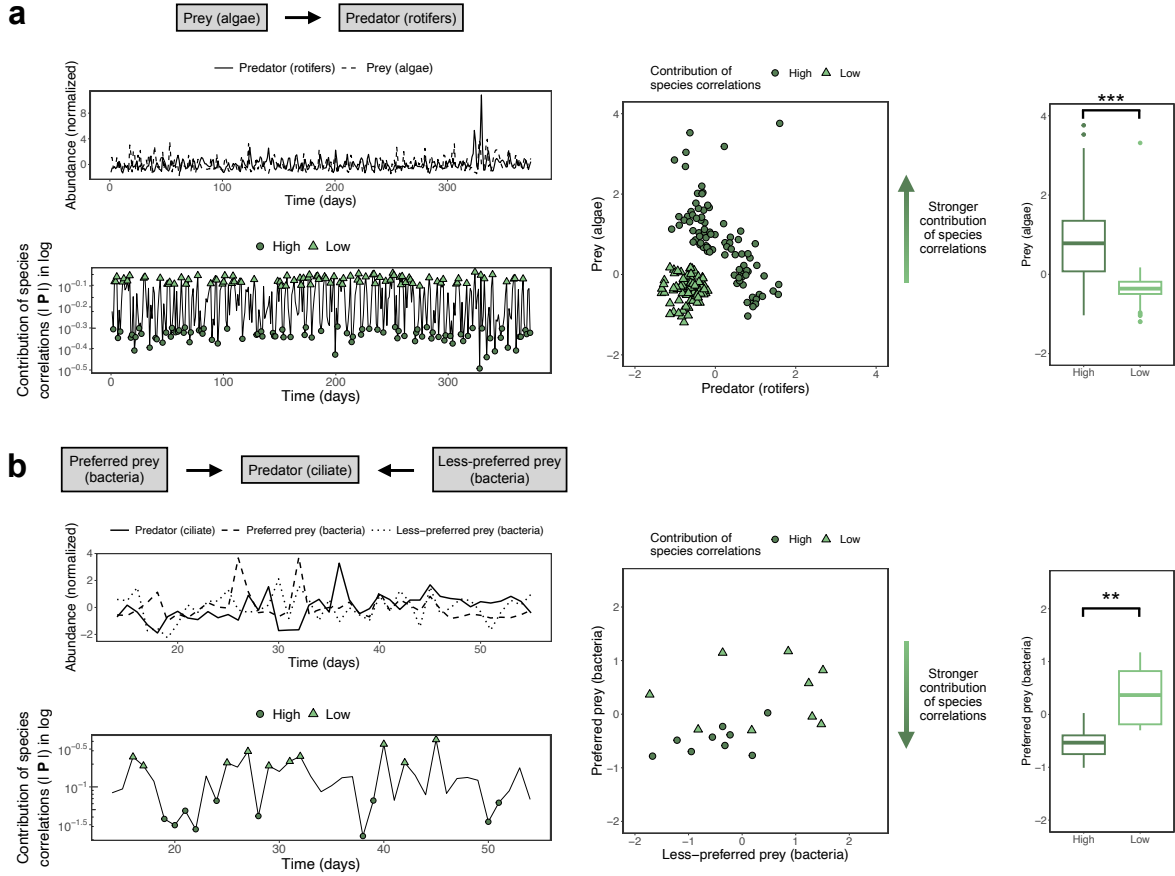


Figure S12. Impact of species correlated responses depends on prey abundance for two experimental communities using time step $k = 3$ instead of $k = 1$. This figure is similar to Figure 5 in the main text, but here we use $k = 3$ instead of $k = 1$ to compute the covariance matrix Σ , which is in turn used to compute the contribution of species correlations ($\log |P|$). Note that results are qualitatively the same as in Figure 5. For the 2-species community (a), prey abundance is higher when the contribution of species correlations is high than when it is low (two sample t-test: $t(130.52) = 9.91$, $p < 0.0001$; data from Blasius et al. (2020)). For the 3-species community, the abundance of the preferred prey is lower when the contribution of species correlations is high than when it is low (two sample t-test: $t(10.12) = -3.14$, $p = 0.01$; data from Becks et al. (2005)).